Available online at www.sciencedirect.com

ScienceDirect

Geochimica et Cosmochimica Acta 216 (2017) 393–416

Geochimica et Cosmochimica Acta

www.elsevier.com/locate/gca

Empirical constraints on partitioning of platinum group elements between Cr-spinel and primitive terrestrial magmas

Jung-Woo Park [a,*], Vadim Kamenetsky [b,c], Ian Campbell [d], Gyuseung Park [a], Eero Hanski [e], Evgeny Pushkarev [f]

[a] School of Earth and Environmental Sciences & Research Institute of Oceanography, Seoul National University, Seoul 08826, South Korea
[b] School of Physical Sciences, University of Tasmania, Hobart, Tasmania 7001, Australia
[c] Institute of Experimental Mineralogy RAS, Chernogolovka 142432, Russia
[d] Research School of Earth Sciences, Australian National University, Canberra, ACT 2601, Australia
[e] Oulu Mining School, P.O. Box 3000, 90014 University of Oulu, Finland
[f] Institute of Geology and Geochemistry, Ural Branch of the Russian Academy of Science, Ekaterinburg 620075, Russia

Received 24 November 2016; accepted in revised form 28 May 2017; available online 1 June 2017

Abstract

Recent experimental studies and *in situ* LA-ICP-MS analysis on natural Cr-spinel have shown that Rh and IPGEs (Ir-group platinum group elements: Ru, Ir, Os) are enriched in the lattice of Cr-spinel. However, the factors controlling the partitioning behaviour of these elements are not well constrained. In this study, we report the Rh, IPGE, and trace element contents in primitive Cr-spinel, measured by LA-ICP-MS, from nine volcanic suites covering various tectonic settings including island arc picrites, boninites, large igneous province picrites and mid-ocean ridge basalts. The aim is to understand the factors controlling the enrichment of Rh and IPGEs in Cr-spinels, to estimate empirical partition coefficients between Cr-spinel and silicate melts, and to investigate the role of Cr-spinel fractional crystallization on the PGE geochemistry of primitive magmas during the early stages of fractional crystallization.

There are systematic differences in trace elements, Rh and IPGEs in Cr-spinels from arc-related magmas (Arc Group Cr-spinel), intraplate magmas (Intraplate Group Cr-spinel), and mid-ocean ridge magmas (MORB Group Cr-spinel). Arc Group Cr-spinels are systematically enriched in Sc, Co and Mn and depleted in Ni compared to the MORB Group Cr-spinels. Intraplate Group Cr-spinels are distinguished from the Arc Group Cr-spinels by their high Ni contents. Both the Arc and Intraplate Group Cr-spinels have total Rh and IPGE contents of 22–689 ppb whereas the MORB Group Cr-spinels are depleted in Rh and IPGE (total < 20 ppb). Palladium and Pt contents are below detection limit for all of the studied Cr-spinels ($<$1–5 ppb). The time-resolved spectra of LA-ICP-MS data for Cr-spinels mostly show constant count rates for trace element and Rh and IPGEs, suggesting homogeneous distribution of these elements in Cr-spinels. The PGE spikes observed in several Cr-spinels were interpreted to be PGE-bearing mineral inclusions and excluded from calculating the PGE contents of the Cr-spinels.

On primitive mantle normalized diagrams the Arc Group Cr-spinels are characterized by a fractionated pattern with high Rh and low Os. The Intraplate Group Cr-spinels show flat patterns with positive Ru anomalies. Our results, together with the experimental and empirical data from previous studies, show that PGE patterns of Cr-spinel largely mimic that of the rock in which they are found, and that Rh, Ir and Os contents increase with increasing Fe^{3+} contents (i.e. magnetite component) in Cr-spinel, although Ru does not. These observations suggest that the enrichment of Rh and IPGEs in Cr-spinel is controlled by a combination of the Rh and IPGE contents in parental melts and the magnetite component of the spinel. Empirical partition coefficients (D) for Rh and IPGEs between Cr-spinels and silicate melts were calculated using the Rh and IPGE contents

* Corresponding author.
E-mail address: jung-woo.park@snu.ac.kr (J.-W. Park).

http://dx.doi.org/10.1016/j.gca.2017.05.039

of the Cr-spinel and their host volcanic rocks after subtracting the accumulation effect of Cr-spinel. The *D* values for the Intraplate and MORB Group Cr-spinels increase with increasing magnetite component in Cr-spinel and range from 6 to 512, which is consistent with previously reported experimental and empirical values. In contrast, the Arc Group Cr-spinels have significantly higher *D* values (e.g. up to ~3700 for Ru) than those of the Intraplate and MORB Group at the same magnetite concentration in the Cr-spinel, suggesting Rh and IPGEs dissolved in silicate melt have stronger affinity for Cr spinel under arc magma conditions than in intraplate magmas. This may be partly attributed to the low temperature of arc magmas relative to intraplate magmas, which leads to the Arc Group Cr-spinels having more octahedral sites at the same magnetite components than the Intraplate Group Cr-spinels. Because of significantly higher *D* values for the Arc Group Cr-spinels, compared with the Intraplate Group and MORB Group spinels, fractional crystallization of Cr-spinel will more efficiently fractionate Rh and IPGE from Pd and Pt in arc systems than in intraplate and MORB systems, which accounts for the highly fractionated PGE patterns in arc basalts.

Keywords: Platinum group elements; Cr-spinel; Partition coefficient; Arc magma; Intraplate magma; Mid ocean ridge magma

1. INTRODUCTION

All terrestrial magmas contain higher concentrations of PPGEs (Pd-group platinum group elements: Pd, Pt, Rh) relative to IPGEs (Ir-group platinum group elements: Ir, Ru, Os). As a consequence, they show fractionated primitive mantle normalized PGE patterns with $Pd_N/Ir_N \gg 1$, although the magnitude of fractionation varies with magma types. Various mineral phases are suggested to account for the fractionation during partial melting and fractional crystallization (Barnes et al., 1985). These phases include monosulfide solid solution, platinum group minerals and olivine, but recently the role of Cr-spinel has attracted increasing attention.

Cr-spinel is a common early-crystallizing mineral in most primitive terrestrial magmas. Therefore, its chemistry reflects the primitive magma composition from which it crystallizes and its composition provides useful information on the nature of its parent magma (e.g. Barnes and Roeder, 2001; Kamenetsky et al., 2001). The influence of Cr-spinel fractional crystallization on platinum group element (PGE) geochemistry has been debated recently. Positive correlations between Cr and PGE contents in volcanic rocks (e.g. Hamlyn et al., 1985), and the significant enrichment of PGE in cumulus rocks with abundant Cr-spinel (e.g. Page et al., 1984), have suggested that Cr-spinel may be an important host mineral for PGEs. However, it has been unclear whether these elements are in solid solution in Cr-spinel or hosted by PGE-bearing mineral (PGM) inclusions within Cr-spinel phenocrysts.

Early studies suggested that PGE cluster or micronugget hosted by Cr-spinels play more important role in fractionation of PGE (Tredoux et al., 1995; Ballhaus and Sylvester, 2000). Fiorentini et al. (2004) investigated Cr-spinels from komatiitic basalts from the Agnew-Wiluna Belt, Australia using *in situ* laser ablation (LA)-ICP-MS. They attributed the abundant Ir-Os or Pt spikes in LA-ICP-MS time-resolved depth profiles of some Cr-spinels to presence of PGM inclusions.

However, recent LA-ICP-MS studies of volcanic Cr-spinel have shown that significant amounts of Rh and IPGEs are homogeneously distributed in Cr-spinel at the sub-micrometer scale, suggesting that they are held in the crystal lattice. Locmelis et al. (2011) reported that komatiitic Cr-spinels from the Yilgarn Craton, Australia contain 200–500 ppb of Ru. Park et al. (2012) measured the PGE contents of Cr-spinels from the oxidized Ambae arc picrites and showed that they contain average concentrations of 78 ppb Rh, 96 ppb Ru, 44 ppb Ir and 40 ppb Os, which are at least an order of magnitude higher than those in the whole-rock picrite samples in which they were found. Pagé et al. (2012) and Pagé and Barnes (2016) investigated Cr-spinels from various rock types including komatiite, boninite, oceanic island tholeiitic basalt (OIB), continental flood basalt (CFB) and mid-ocean ridge basalt (MORB) and found that they all have tens of ppb Rh and IPGEs, except for the MORB Cr-spinels, which are depleted in PGEs (<13 ppb). Arguin et al. (2016) studied Cr-spinels from Emeishan picrites and reported 20–30 ppb of Rh, Ir and Os and ~250 ppb of Ru in the Cr-spinel. Kamenetsky et al. (2015) showed that Cr-spinels from an oxidized Siberia meimechite have 11 ppb Rh, 240 ppb Ru, 51 ppb Ir, and 91 ppb Os whereas those from the reduced Uralian ankaramites are less enriched in these elements with 60–70 ppb Rh and Ru and <10 ppb Ir and Os. The enrichment of Rh and IPGEs in volcanic Cr-spinels is consistent with experimental studies of spinel phases (Capobianco and Drake, 1990, 1994; Righter et al., 2004; Brenan et al., 2012). Palladium and Pt contents were both below the detection limit of LA-ICP-MS in all of these studies (7 ppb Pd and 6 ppb Pt; Park et al., 2012), which was attributed to charge mismatch and the different ionic radius for Pd and crystal configuration for Pt (Brenan et al., 2012).

Brenan et al. (2012) suggested that one of the major controlling factors for partitioning of Rh, Ru and Ir into Cr-spinel is the availability of the divalent octahedral site in the spinel structure. As PGEs have a high octahedral site preference energy, they preferentially partition into the octahedral sites in the spinel structure (Brenan et al., 2012 and references therein). As a consequence, divalent Rh, Ir and possibly some Ru substitute Fe^{2+} or Mg^{2+} in the octahedral sites. Pure chromite has a normal-spinel structure with no divalent octahedral sites, but as the proportion of the magnetite component increases in the spinel the fraction of the divalent octahedral sites increases, and hence the

partition coefficients of Rh and IPGEs also increase. Brenan et al. (2012) confirmed this hypothesis by a high temperature (>1400 °C) experimental study of the partitioning of Rh, Ru and Ir between Cr-spinel and silicate melts and found positive correlations between the ferric iron contents in the Cr-spinel and the partition coefficients for these elements. A similar phenomenon was observed from the study of natural Cr-spinels. Park et al. (2012) measured PGE contents in Cr-spinel from highly oxidized arc magmas and reported that the Rh, Ru and Os contents increase as the magnetite component of the Cr-spinel increases. However, when Cr-spinels from different magmatic systems are compared, this correlation is not apparent (Pagé and Barnes, 2016), which implies other factors, such as temperature, the PGE solubility in silicate melts and magma composition might be more important for partitioning of PGEs in Cr-spinel than the magnetite component. It should also be noted that the PGE contents of Cr-spinels might also be affected by sub-solidus re-equilibration and subsequent PGM exsolution (e.g. Park et al., 2012; Barnes et al., 2016; Pagé and Barnes, 2016).

In this study, we have measured the PGE and trace element contents of Cr-spinels from diverse magmatic suites using the *in situ* LA-ICP-MS technique. The aims of this study are: (1) to constrain the factors for Rh and IPGE enrichment in Cr-spinel, (2) to estimate empirical partition coefficients for Rh and IPGEs between Cr-spinel and silicate melts, and (3) to understand the effect of Cr-spinel crystallization on PGE geochemistry in terrestrial magmatic systems.

2. SAMPLE DESCRIPTION

We have measured PGE and trace element contents in Cr-spinels from nine volcanic suites. Volcanic rocks from diverse tectonic settings were selected, which include: a high-K island arc picrite from the Eastern Kamchatka (Kamenetsky et al., 1995); a boninitic picrite from the Margi area of the Troodos ophiolite, Cyprus (Cameron, 1985); an arc ankaramite from the Urals, Russia; tholeiitic picrites from West Greenland (Holm et al., 1993) and the Emeishan large igneous province, China (Hanski et al., 2010; Kamenetsky et al., 2012); two komatiites and a picritic basalt from Finland (Hanski et al., 2001); mid-ocean ridge basalts from the Mid-Atlantic Ridge (MAR) at 43° N (Shibata et al., 1979; Kamenetsky and Crawford, 1998), the project FAMOUS area (the French-American Mid-Ocean Undersea Study; Langmuir et al., 1977; Kamenetsky, 1996), and the Macquarie Island, SW Pacific (Husen et al., 2016). The most primitive samples were selected where possible to ensure that the analysed Cr-spinels reflect the primitive magma composition with minimal chemical variations due to fractional crystallization. These samples, together with the samples from literatures (Locmelis et al., 2011; Park et al., 2012; Kamenetsky et al., 2015; Pagé and Barnes, 2016; Arguin et al., 2016) show a wide range in major element compositions, especially in Fe^{3+}/R^{3+} ($Fe^{3+}/(Fe^{3+} + Cr^{3+} + Al^{3+})$), which has enabled us to investigate the influence of the Cr-spinel composition on the partitioning of PGEs and other trace elements between Cr-spinel and silicate melts. In this study, we divided the Cr-spinels into three groups: Arc, Intraplate and MORB Groups based on their tectonic settings.

2.1. Arc magmatism

2.1.1. Kamchatka picrite

Sample Ty-24 is from the Tumrok Range, Eastern Kamchatka (Kamenetsky et al., 1995), which is a thick (up to ~1.2 km) late Cretaceous and Paleogene picrite-basalt volcanic succession. The picrite has a glassy matrix with skeletal clinopyroxene and amphibole crystals. Cr-spinel occurs mostly as inclusions in olivine phenocrysts with Fo contents that range from 85 to 94 mol% (Kamenetsky et al., 1995).

2.1.2. Troodos picrite

One sample from the Upper Pillow Lavas in the Margi area of the Troodos Massif was selected for analyses. The Upper Pillow Lavas occur as a narrow, discontinuous belt that surrounds the Troodos Massif. Most of the picrites from the Margi area have a glassy matrix and olivine microphenocrysts with Fo contents of 90–92 mol% (Cameron, 1985). The Margi Cr-spinels have compositions close to magnesiochromite and occur as inclusions in olivine or euhedral microphenocrysts in the groundmass with a grain size of ~50 μm (Cameron, 1985).

2.1.3. Urals ankaramite

Sample Pe1023 is a part of a large lava bomb within a tuff deposit of the Gadel'sha paleovolcano, which belongs to the Irendyk volcanic formation in the Magnitogorsk island arc zone in the Southern Urals. It is a highly clinopyroxene-phyric volcanic rock with 30–35% of clinopyroxene phenocrysts (Mg# = 0.90–0.93), 3–10 mm in size. Rare olivine phenocrysts, which range in size from 5 to 10 mm, are completely replaced by secondary minerals. Cr-spinel forms 0.5–1 mm-sized idiomorphic microphenocrysts in the groundmass or more often in the former olivine phenocrysts.

2.2. Intraplate magmatism

2.2.1. Greenland tholeiitic picrite

The olivine-phyric rock selected for this study represents typical picritic lavas belonging to the Paleocene Vaigat Formation in West Greenland (Holm et al., 1993; Larsen and Pedersen, 2000). Abundant olivine (86–92 mol% Fo) and rare Cr-spinel phenocrysts are set in a glassy matrix.

2.2.2. Emeishan picrite, China

The tholeiitic basalts from the Emeishan Large Igneous Province are subdivided into two groups: high-Ti and low-Ti basalts (Xu et al., 2001). We have analysed Cr-spinels from three picrite samples from the Emeishan Large Igneous Province, China. One sample (EM-43) from the Binchuan area is associated with low-Ti basalts (Kamenetsky et al., 2012). The other two samples (9EJH-06 and 10EJH-06) are from the Lijiang area where massive picrite lavas occur as ~40 m thick intercalations in the lower parts of a 5.5-km-thick succession of pyroxene-phyric high-Ti basalts (Hanski et al., 2010).

2.2.3. Paleoproterozoic komatiite, Finland

We have analysed Cr-spinel from three samples from the Central Lapland greenstone belt, coming from two different areas located 30 km apart, Jeesiörova (12D-PPR-97 and 17-EJH-97) and Peuramaa (sample 800-46-LVP-86) and occurring as amygdaloidal massive flows or pillow lavas. The Jeesiörova samples can be classified as LREE-depleted Ti-enriched komatiites and the Peuramaa sample as LREE-enriched picritic basalt.

2.3. Mid-ocean ridge magmatism

2.3.1. MORB from the Mid-Atlantic Ridge at 43°N

Sample AII32-12-7 was dredged by the R/V Atlantis II from the 1440 to 1820 m water depth in the median valley of MAR at 42°57′N, 29°10′W (Kamenetsky and Crawford, 1998). It is a porphyritic pillow basalt with ~5 vol.% phenocrysts of olivine and clinopyroxene, in which Cr-spinel occur as inclusions. The host rocks are primitive basalts containing 10–12 wt.% MgO and 13.2–15.2 wt.% CaO (Kamenetsky and Crawford, 1998).

2.3.2. MORB from the FAMOUS area

Samples ARP-73-10-03 and CH31 DR08-136-02 were dredged from the FAMOUS area of the Mid-Atlantic Ridge at 36°50′N (Kamenetsky, 1996). They are olivine phyric picrites, containing olivine phenocrysts with Fo contents of up to 92.1 mol.%. Cr-spinel occurs in a glassy or fine-grained matrix as small crystals and as inclusions in olivine.

2.3.3. MORB from the Macquarie Island, SW Pacific

Macquarie Island (~34 km long and ~5 km wide) is located in the SW Pacific between New Zealand, Tasmania and Antarctica, as an emerged part of the Macquarie Ridge. The island hosts a complete ophiolite section composed of mantle harzburgite, through lower crustal troctolite, wehrlite, dunite and gabbro, to sheeted dykes and pillow lavas. Two picrite samples (SL2 and 60,796) used in this study were taken from lensoidal bodies intercalated with basaltic pillow lavas. They are porphyritic rocks containing euhedral phenocrysts (up to ~30 vol.%) of olivine, Cr-spinel, plagioclase and clinopyroxene. The olivine compositions are primitive with Fo contents up to 91 mol.%. Cr-spinel occurs both in the groundmass and as inclusions in olivine.

3. ANALYTICAL TECHNIQUE

3.1. Mineral major, trace element and PGE analysis

The major element compositions of Cr-spinel in the studied samples were analysed by a Hitachi SU-70 Schottky field emission scanning electron microscope (FE-SEM) fitted with Oxford INCA Energy XMax 80 silicon drift detector energy dispersive X-ray spectrometry system (Central Science Laboratory, University of Tasmania). The results are consistent with previously measured values (Cameron, 1985; Kamenetsky et al., 1995; Kamenetsky, 1996; Kamenetsky and Crawford, 1998; Kamenetsky et al., 2012; Husen et al., 2016), which were obtained using a wave-length dispersive X-ray spectroscopy Camebax electron microprobe (Vernadsky Institute of Geochemistry, Moscow), Cameca SX-50 and Cameca SX-100 (Central Science Laboratory, University of Tasmania), and JEOL Superprobe JXA-8200 (Max Planck Institute for Chemistry, Mainz). In this study, Fe^{3+}/Fe^{2+} of Cr-spinels were estimated based on stoichiometry using the method described in Barnes and Roeder (2001).

Platinum group and trace element contents in Cr-spinel were measured by LA-ICP-MS at Research School of Earth Sciences, Australian National University, using the method described by Park et al. (2012). In summary, the system is composed of a 193 nm excimer laser (Lambda Physik Compex 110) and an Agilent 7700x quadrupole ICP-MS. The analyses were performed using laser beam sizes of 80–105 μm, a pulse rate of 5 Hz, and an energy fluence of ~2.5 J/cm^2. The NIST 612 or 610 glasses were used as external standards for trace elements and the CANMET po727 FeS standard for the PGEs. The composition of the po727 standard is reported in Barnes et al. (2008). The Al and Fe contents, independently obtained by FE-SEM, were used as an internal standard for the trace elements and PGEs respectively to correct the yield differences between the Cr-spinels and the external standards. Data reduction was carried out using an in-house excel spread sheet according to the method of Longerich et al. (1996).

The measured isotopes were ^{24}Mg, ^{27}Al, ^{29}Si, ^{45}Sc, ^{49}Ti, ^{51}V, ^{53}Cr, ^{55}Mn, ^{57}Fe, ^{59}Co, ^{61}Ni, ^{65}Cu, ^{66}Zn, ^{101}Ru, ^{103}Rh, ^{105}Pd, ^{189}Os, ^{192}Os, ^{193}Ir, and ^{195}Pt. The isobaric interference derived from metal oxides (MO^+) and metal argides (MAr^+) were monitored by analyses of pure Cu metal (C-430, Fisher Scientific Company) and synthetic Ni-sulphide. The expected isobaric interferences are around 1.4 ppb Ru per 1000 ppm Ni and 7.7 ppb Rh per 1000 ppm Cu in Cr-spinel, which result in negligible isobaric interferences of ^{61}Ni^{40}Ar + and ^{63}Cu^{40}Ar + on ^{101}Ru and ^{103}Rh (<1.5%) for most samples. Micro inclusions, identified as spikes in time-resolved spectra data, were excluded when calculating the concentrations.

Multiple analyses were performed using the CANMET po727 FeS standard, the NIST 610 and 612 glass standards and an in-house PGE glass standard provided by Guilherme Mallmann. The latter was analysed for quality control. The results are present in Appendix B. The measured PGE and trace element concentrations of the standards agree within two standard deviations with the published or working values (Sylvester and Eggins, 1997; Jochum et al., 2011; Park et al., 2012).

3.2. Whole-rock PGE analysis

The whole-rock PGE contents of samples from three of the volcanic suites were measured: the Urals ankaramite sample (Pe1023), Macquarie Island MORB glass sample (47,979), and Finland komatiite sample 12C-PPR-97 (from the same outcrop as sample 12D-PPR-97) (Table 1). The sample Pe1023 was analysed by a Ni-sulfide fire assay method combined with Te-coprecipitation at Geoscience Laboratories, Canada (Method code: IMP-200). The

Table 1
Whole-rock Cr and PGE compositions.

Locality and type	Sample no.	Cr (ppm)	Pd (ppb)	Pt (ppb)	Rh (ppb)	Ru (ppb)	Ir (ppb)	Os (ppb)
Macquarie Island MORB	47,979	320	0.55	0.57	0.39	0.80	0.53	n.d.
Urals ankaramite	Pe-1023	280	7.7	19.8	0.70	0.34	0.20	n.d.
Finland komatiite	12C-PPR-97	3742	11.6	20.9	1.07	4.36	3.05	2.73

n.d., Not determined.

method determination limits are 0.4 ppb for Au, 0.12 ppb for Pd, 0.17 ppb for Pt, 0.04 ppb for Rh, 0.08 ppb for Ru, 0.01 ppb for Ir. The measured PGE contents in sample Pe1023 are 0.88 ppb Au, 7.69 ppb Pd, 19.8 ppb Pt, 0.7 ppb Rh, 0.34 ppb Ru, 0.2 ppb Ir. The Macquarie Island MORB was analysed by the Ni-sulfide fire assay – isotope dilution method of Park et al. (2012). Rh concentration was determined by the method of Meisel et al. (2003) using count rates of ^{103}Rh and ^{106}Pd with assumption that loss of Rh during the analytical procedure was similar to that of Pd. The detection limits are 12 ppt Ir, 1 ppt Ru and 3 ppt Rh. The Ir, Ru and Rh contents in sample 47,979 are 0.53 ppb, 0.80 ppb and 0.39 ppb, respectively. The komatiite sample 12C-PPR-97 was analysed for PGEs using Ni-sulfide fire assay followed by Te co-precipitation and measurement by ICP-MS at the Geological Survey of Finland. Their concentrations are Os 2.73 ppb, Ir 3.05 ppb, Ru 4.36 ppb, Rh 1.07 ppb, Pt 20.9 ppb, Pd 11.6 ppb.

4. RESULTS

4.1. Major element compositions

Major element compositions of Cr-spinels in the studied rocks are presented in Table 2 and Fig. 1. The Arc Group Cr-spinels from the Kamchatka picrite, Troodos picrite and Urals ankaramite are characterized by low Al_2O_3 and TiO_2 contents (Fig. 1a). The Fe^{3+}/R^{3+} of the Kamchatka Cr-spinels ranges from 0.10 to 0.23 which is significantly higher than in Cr-spinels from the other localities at similar Mg#, suggesting strongly oxidized conditions during their crystallization (Fig. 1b). The Fe^{3+}/R^{3+} ratios in Cr-spinels from the Troodos picrite and Urals ankaramite are ~0.05 and ~0.08, respectively, which are relatively low. The average Cr# and Mg# values of the Cr-spinel from the Kamchatka and Troodos picrite are >0.72 and >0.60, respectively (Table 2). These are similar to those of the most primitive Cr-spinel in each picrite suite (Cameron, 1985; Kamenetsky et al., 1995). The average Cr# and Mg# values of the Urals ankaramite are 0.82 and 0.55 respectively.

The Intraplate Group Cr-spinels from the West Greenland and Emeishan igneous provinces have slightly higher average Al_2O_3 and TiO_2 contents than the Arc Group Cr-spinels analysed in this study (Fig. 1a). The Emeishan Cr-spinel compositions can be divided into two sub-groups. Those from the high-Ti picrites (9EJH-06 and 10EJH-06) contain higher TiO_2 and lower Al_2O_3 and plot in the OIB field. The Cr-spinels from the low-Ti picrites (EM-43) contain low TiO_2 (~0.54 wt.%), reflecting the composition of the magma from which they crystallized (Fig. 1a). Both the Greenland and Emeishan Cr-spinels are characterized by relatively low Mg# of ~0.54 and intermediate Fe^{3+}/R^{3+} of ~0.1 (Fig 1b). The Finland komatiite and picritic basalt Cr-spinels have very similar major element compositions in spite of the significant differences in their REE and large ion lithophile element contents in host volcanic rocks (Hanski et al., 2001; Hanski and Kamenetsky, 2013). They have average Mg# of 0.66 and 0.60 and Fe^{3+}/R^{3+} of 0.07 and 0.09, respectively (Fig. 1; Table 2).

The MORB Group Cr-spinel from the MAR at 43°N, the FAMOUS area and the Macquarie Island are characterized by significantly high Al_2O_3 contents (avg. >20 wt. %), the lowest Fe^{3+}/R^{3+} (avg. <0.05) and low Cr# (avg. <0.59) that reflect crystallization from a reduced Al-rich melt (Fig. 1; Table 2).

4.2. Trace element compositions

The trace element contents of the Cr-spinels are presented in Table 3, Fig. 2 and Appendix B. Fig. 2 shows a comparison of trace element compositions for the volcanic Cr-spinels normalized to average composition of the Cr-spinels from the Eastern Pacific Rise (EPR) MORB reported in Pagé and Barnes (2009). We changed the order of elements from Pagé and Barnes (2009) to clarify the compositional differences between Arc, Intraplate and MORB Group Cr-spinels.

The Arc Group Cr-spinels from the Kamchatka and Troodos picrites and Urals ankaramite are characterized by fractionated patterns with about 1.5 times enriched in Sc, Mn, and Co and are depleted in Ni a factor of 2 compared to the EPR MORB Cr-spinels (Fig. 2; Pagé and Barnes, 2009). These trends are consistent with the trace element characteristics of Cr-spinel from other arc-related magmatic systems: the Ambae picrite (Park et al., 2012), and the boninites from the Thetford Mines Ophiolite (Québec) and Bonin Island (Pagé and Barnes, 2009). Vanadium and Zn contents are variable. They are relatively enriched in Cr-spinels from boninites compared with those from arc picrites.

The Intraplate Group Cr-spinels from the Greenland and Emeishan picrites and the Finland komatiites and picritic basalts, also show fractionated patterns with slight enrichment of Sc, Mn, Co and Zn, and depletion of Ni compared to the EPR MORB Cr-spinel (Fig. 2). The compositions of MORB Cr-spinels from Mid-Atlantic Ridge at 43°N, FAMOUS area, and Macquarie Island in this study are similar to the EPR MORB Cr-spinels (Pagé and Barnes, 2009) in most trace elements, but about a factor of 2 lower in Zn and Ni.

Table 2
Average major element composition of the Cr-spinel (wt.%).

Rock type and locality	Sample no.	*n*	Cr_2O_3	Al_2O_3	TiO_2[a]	FeO	Fe_2O_3[b]	MgO	Total	Fe^{2+}/Fe^{3+}	$Fe^{3+}/\sum Fe$	Mg#	Cr#	Cr^{3+}/R^{3+}	Fe^{3+}/R^{3+}	Al^{3+}/R^{3+}
Arc Group Cr-spinel																
Kamchatka picrite	TY-24	9 avg.	50.6	11.1	0.33	12.7	10.7	13.7	99.2	1.36	0.43	0.66	0.75	0.65	0.13	0.21
		1σ	2.8	1.3	0.07	2.1	3.2	1.5	0.3	0.18	0.03	0.06	0.02	0.03	0.04	0.05
Urals ankaramite	Pe1023	5 avg.	56.7	8.6	0.32	16.1	6.0	11.3	99.0	2.99	0.26	0.55	0.82	0.75	0.08	0.17
		1σ	2.7	1.4	0.08	3.5	0.9	2.3	0.6	0.70	0.04	0.11	0.03	0.04	0.01	0.04
Troodos picrite	Margi	9 avg.	52.9	13.8	0.36	15.3	4.5	12.4	99.3	3.78	0.21	0.59	0.72	0.68	0.06	0.26
		1σ	1.4	1.0	0.05	1.6	0.3	1.0	0.3	0.33	0.02	0.04	0.02	0.02	0.00	0.02
Intraplate Group Cr-spinel																
Greenland picrite	2142	7 avg.	41.2	18.8	0.93	19.2	8.5	10.7	99.2	2.66	0.28	0.50	0.60	0.53	0.11	0.36
		1σ	3.3	2.3	0.14	2.1	2.5	1.4	0.5	0.69	0.06	0.06	0.04	0.04	0.03	0.05
Emeishan picrite (High-Ti)	9EJH-06, 10EJH-06	11 avg.	48.3	11.7	1.61	19.3	7.8	10.2	98.8	2.76	0.27	0.49	0.74	0.66	0.10	0.24
		1σ	1.3	0.5	0.15	2.1	0.6	1.4	0.3	0.26	0.02	0.06	0.01	0.01	0.01	0.01
Emeishan picrite (Low-Ti)	EM-43	4 avg.	47.0	15.0	0.54	19.3	6.9	9.9	98.6	3.17	0.24	0.48	0.68	0.62	0.09	0.29
		1σ	1.8	1.4	0.05	0.5	1.0	0.4	0.3	0.54	0.03	0.02	0.03	0.03	0.01	0.03
Finland komatiite	12D-PPR-97, 17A-EJH-97	12 avg.	52.6	13.7	0.6	13.0	5.6	14.1	99.5	2.64	0.28	0.66	0.72	0.67	0.07	0.26
		1σ	2.4	0.8	0.1	3.1	1.4	2.1	0.4	0.60	0.04	0.09	0.02	0.02	0.02	0.01
Finland picritic basalt	800-Y6-LVP-86	6 avg.	51.0	12.2	1.2	15.3	6.8	12.7	99.2	2.55	0.29	0.60	0.74	0.67	0.09	0.24
		1σ	2.3	0.5	0.2	2.3	1.3	1.5	0.6	0.64	0.04	0.06	0.02	0.02	0.02	0.01
MORB Group Cr-spinel																
MAR, 43°N MORB	All32-12-2	5 avg.	46.4	21.7	0.44	11.3	3.9	16.0	99.6	3.25	0.24	0.72	0.59	0.56	0.04	0.39
		1σ	0.7	1.1	0.06	0.7	0.5	0.5	0.3	0.28	0.02	0.02	0.02	0.01	0.01	0.01
Macquarie Island MORB	SL2, 60,796	10 avg.	41.3	25.8	0.50	12.8	4.1	15.5	100.1	3.47	0.22	0.68	0.52	0.49	0.05	0.46
		1σ	0.9	0.9	0.06	0.5	0.4	0.4	0.2	0.34	0.02	0.01	0.01	0.01	0.00	0.01
FAMOUS MORB	ARP 73-10-03, CH31 PR08-136-02	8 avg.	40.6	27.7	0.26	10.8	3.3	16.8	99.4	3.61	0.22	0.73	0.50	0.48	0.04	0.49
		1σ	0.9	0.8	0.02	0.4	0.3	0.2	0.1	0.38	0.02	0.01	0.01	0.01	0.00	0.01

[a] TiO_2 concentrations below 0.6 wt.% were measured by LA-ICP-MS.
[b] Obtained by stoichiometric calculations using the equations of Barnes and Roeder (2001).

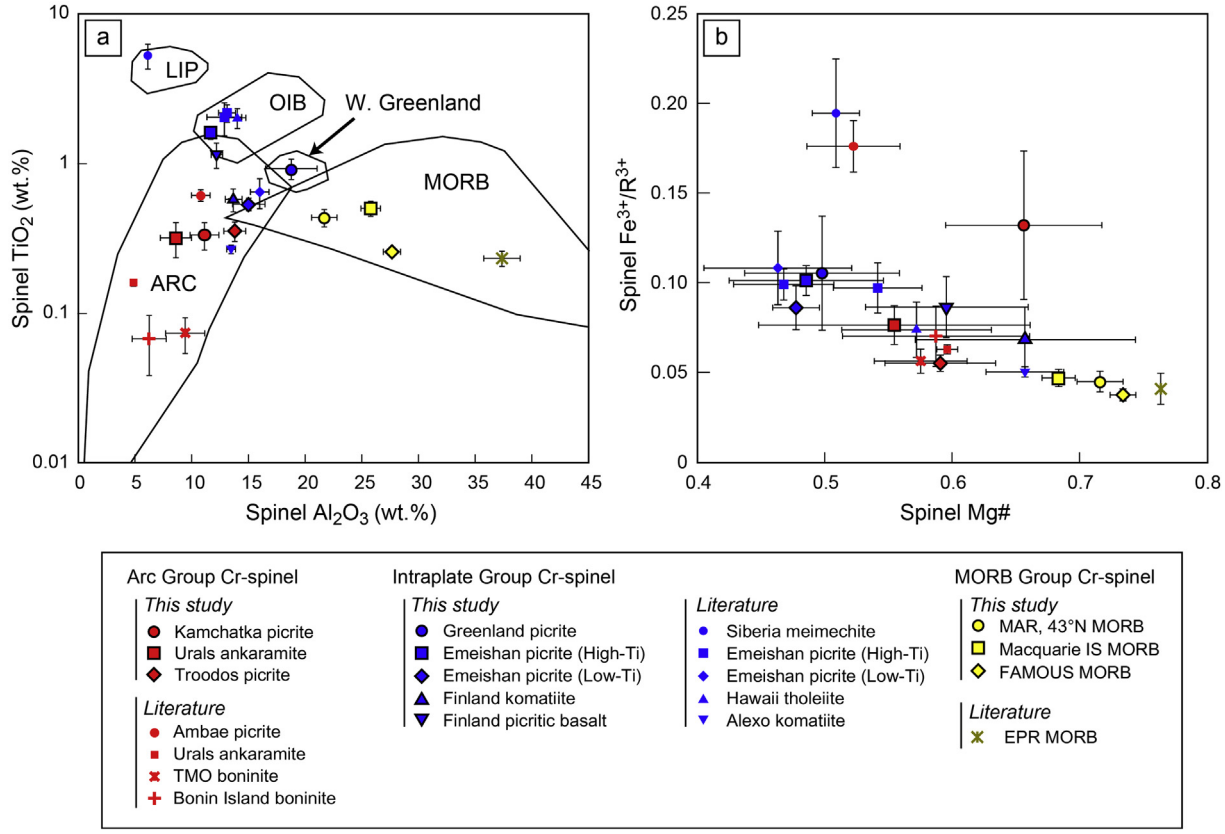

Fig. 1. Major element compositions of Cr-spinel. (a) Binary plot of TiO_2 against Al_2O_3. Fields for Cr-spinel from various tectonic settings are from Kamenetsky et al. (2001). Note that a field for LIP (Large Igneous Province) Cr-spinels is restricted to Cr-spinels enclosed in olivine, which is smaller than that of Barnes and Roeder (2001). (b) Binary plot of Fe^{3+}/R^{3+} against Mg#. The error bars are one standard deviation of multiple analyses for Cr-spinel from each locality. The compositions of Cr-spinel reported in literature are from Park et al. (2012), Kamenetsky et al. (2015) and Pagé and Barnes (2016).

4.3. Platinum group element compositions

The average PGE abundances of the studied Cr-spinels are shown in Table 3 and Figs. 3–8, 10 and 11, with the full data reported in Appendix B. Most of the Cr-spinels have concentrations of Ru (up to 423 ppb), Rh (up to 173 ppb), Os (up to 80 ppb), and Ir (up to 191 ppb) that are well above the detection limits of LA-ICP-MS (Table 3). However, the MORB Group Cr-spinels are characterized by low PGE contents, which are close to or slightly above the detection limits (~1–10 ppb). Palladium, Pt and Re were not detected by LA-ICP-MS in any of analysed Cr-spinel. Fig. 3 shows a representative time-resolved spectrum for two Cr-spinel grains analysed by LA-ICP-MS. The counts for Rh and IPGEs were uniform during ablation, showing a homogeneous distribution of these elements within the spatial resolution of the LA-ICP-MS analysis (Fig. 3a). PGE-rich inclusions in some Cr-spinel grains were identified as spikes in the time-resolved spectra (Fig. 3b; Appendix B). These spikes were most abundant in the Cr-spinels from the Kamchatka picrite, with 4 out of 10 analyses showing Pt ± Ir ± Os spikes. They were excluded when calculating the PGE contents of the Cr-spinel.

The average PGE contents of the Cr-spinels from each locality are normalized to primitive mantle (PM) values in Fig. 4. The Arc Group Cr-spinels are characterized by fractionated Rh and IPGE patterns with relatively high Rh and low Os contents. These features are consistent with observations from the Cr-spinels from other arc-related magmas, the Ambae picrite, Bonin Island and Thetford Mines Ophiolite boninite (Park et al., 2012; Pagé and Barnes, 2016). The Intraplate Group Cr-spinels show surprisingly similar Rh and IPGE trends, which are characterized by zigzag patterns with relatively enriched Ru and depleted Ir contents compared to Rh and Os. Such patterns are similar to the patterns of the Cr-spinel from the Alexo komatiite, Hawaiian tholeiite, Siberia meimechite and Emeishan picrite (Kamenetsky et al., 2015; Arguin et al., 2016; Pagé and Barnes, 2016). The MORB Group Cr-spinels are PGE-poor. The Arc Group and Intraplate Group Cr-spinels are clearly distinguished in a binary diagram of Rh_N/Ru_N vs. Ir_N/Os_N (Fig. 5a).

The Rh and IPGE patterns of Cr-spinels from a given suite are sub-parallel to each other except for the Kamchatka picrite sample (Fig. 6). Several Cr-spinel grains from this suite show distinctive patterns characterized by positive or negative Ir anomaly and differ from the majority of the

Table 3
Average trace element and PGE composition of the Cr-spinel measured by LA-ICP-MS.

Rock type and locality	Sample no.	*n*	Sc	Ti	V	Mn	Co	Ni	Cu	Zn	Ru	Rh	Pd	Re	Os	Ir	Pt
Arc Group Cr-spinel																	
Kamchatka picrite	TY-24	10 avg.	9	1991	350	1250	176	727	8	314	185	95	<3	n.a.	40	101	<1
		1σ	2	395	41	210	14	113	2	84	93	31			13	60	
Urals ankaramite	Pe1023	5 avg.	7	1921	699	1824	215	333	15	632	6[a]	56	<3	<2	4[a]	6	<1
		1σ	2	506	88	426	21	85	7	363	3	11			3	4	
Troodos picrite	Margi	9 avg.	6	2131	859	1323	201	612	7	445	87	24	<3	<2	5[a]	14	<1
		1σ	0.3	315	144	90	6	65	1	82	31	8			3	6	
Intraplate Group Cr-spinel																	
Greenland picrite	2142	8 avg.	6	4595	774	1704	214	1350	104	747	172	9	<5	n.a.	54	26	<4
		1σ	1	820	218	441	38	170	129	256	33	3			14	6	
Emeishan picrite (High-Ti)	9EJH-06, 10EJH-06	14 avg.	7	9950	756	1476	194	1138	42	531	206	15	<3	<2	38	23	<1
		1σ	1	1160	96	200	10	166	43	135	40	2			15	7	
Emeishan picrite (Low-Ti)	EM-43	4 avg.	6	3063	589	2049	216	987	43	825	336	31	<5	n.a.	20	22	<2
		1σ	2	214	70	108	13	79	24	107	19	3			6	4	
Finland komatiite	12D-PPR-97, 17A-EJH-97	12 avg.	7	3456	649	1054	183	1249	9	281	246	13	<3	<2	43	30	<1
		1σ	1	614	134	245	26	230	5	107	29	5			18	11	
Finland picritic basalt	800-Y6-LVP-86	6 avg.	7	6915	765	1163	187	1208	12	350	231	7	<3	<2	36	20	<1
		1σ	1	1359	211	165	17	190	3	83	41	3			13	5	
MORB Group Cr-spinel																	
MAR, 43°N MORB	All32-12-2	8 avg.	6	2997	763	936	164	929	8	296	<10	3[a]	<3	<2	<4	2[a]	<1
		1σ	1	581	72	89	8	65	3	14		1				1	
Macquarie Island MORB	SL2, 60,796	10 avg.	6	3022	856	920	175	878	6	389	<10	3[a]	<3	<2	4[a]	6[a]	<1
		1σ	2	339	56	49	10	93	1	31		1			3	3	
FAMOUS MORB	ARP 73-10-03, CH31 PR08-136-02	10 avg.	5	1546	934	844	167	931	5	307	<10	<2	<3	<2	<4	<1	<1
		1σ	0.1	101	48	36	4	147	1	26							

Trace elements are in ppm and PGE are in ppb.
n.a., Not analyzed.
[a] Half of the detection limit values were used for some analyses for calculating average PGE concentrations.

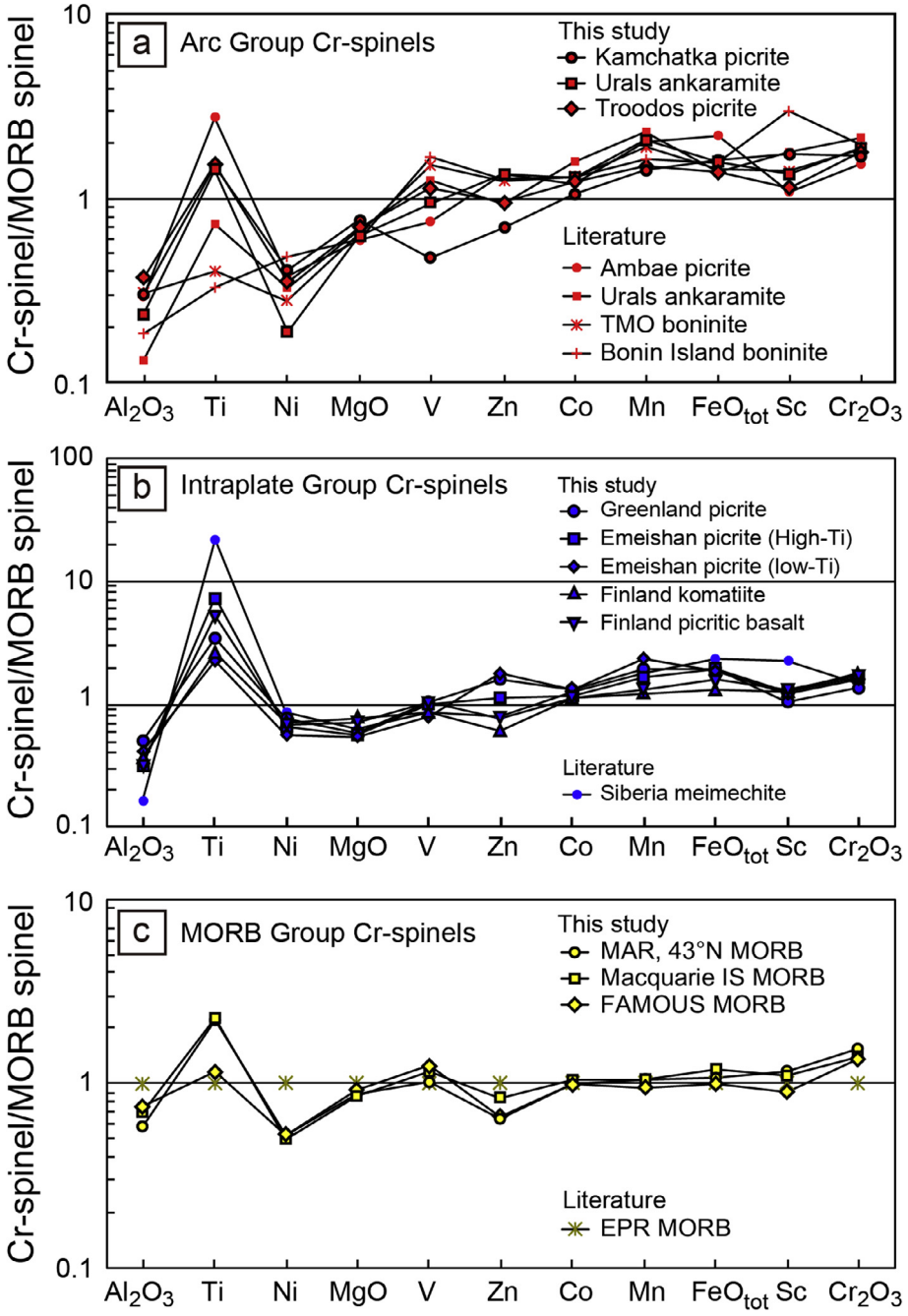

Fig. 2. Trace element compositions of (a) the Arc Group, (b) the Intraplate, and (c) MORB Group Cr-spinels normalized by the EPR MORB Cr-spinel of Pagé and Barnes (2009). The compositions of Cr-spinel reported in literature are from Park et al. (2012), Kamenetsky et al. (2015) and Pagé and Barnes (2009).

analysed spinel crystals (Fig. 6a). Such large Ir variations, compared to other Rh and IPGEs, were also observed in the Cr-spinels from the Ambae picrite (Park et al., 2012). Park et al. (2012) attributed it to co-crystallization of an Ir-bearing Pt-alloy with the Cr-spinel.

The Cr-spinels from the Emeishan high-Ti and low-Ti picrites have slightly different Rh and PGE patterns (Fig. 6d and e). The Cr-spinels from the former contain relatively less Rh and Ru than those from the latter. Similar PGE abundances and systematics have been also reported by Arguin et al. (2016). The Rh-IPGE patterns for Cr-spinels from the Finland komatiite and picritic basalt do not exhibit discernible differences (Fig. 6f).

Iridium and Os in the studied Cr-spinel show overall positive correlations with Fe^{3+}/R^{3+} whereas Ru does not (Fig. 7a–c). Similar trends were also observed in Park et al. (2012) and Pagé and Barnes (2016). Rhodium exhibits a positive correlation with Fe^{3+}/R^{3+} for the Arc Group

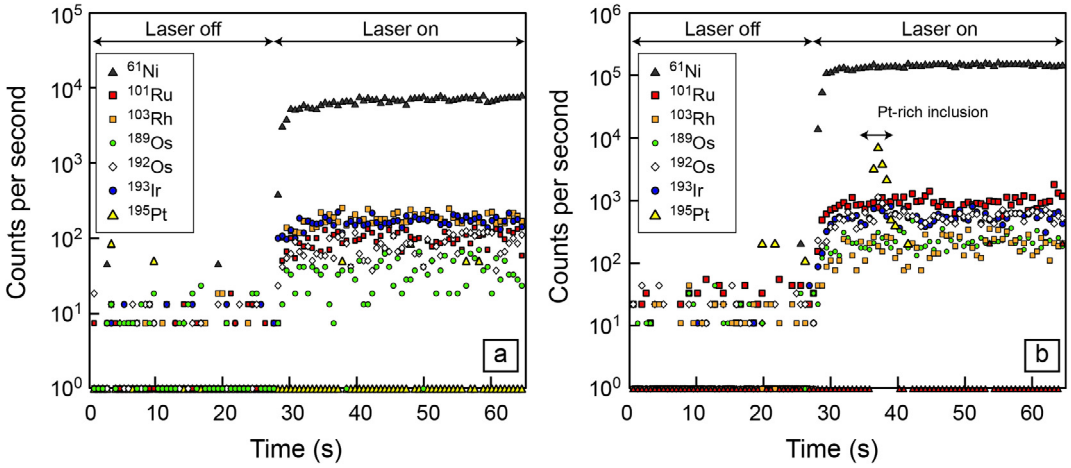

Fig. 3. Representative time-resolved spectra of LA-ICP-MS analyses on Cr-spinel from (a) sample Ty-24, the Kamchatka arc picrite and (b) sample 1656, the Siberia meimechite (Kamenetsky et al., 2015). A Pt spike indicates presence of a Pt-bearing micro-inclusion in the Cr-spinel.

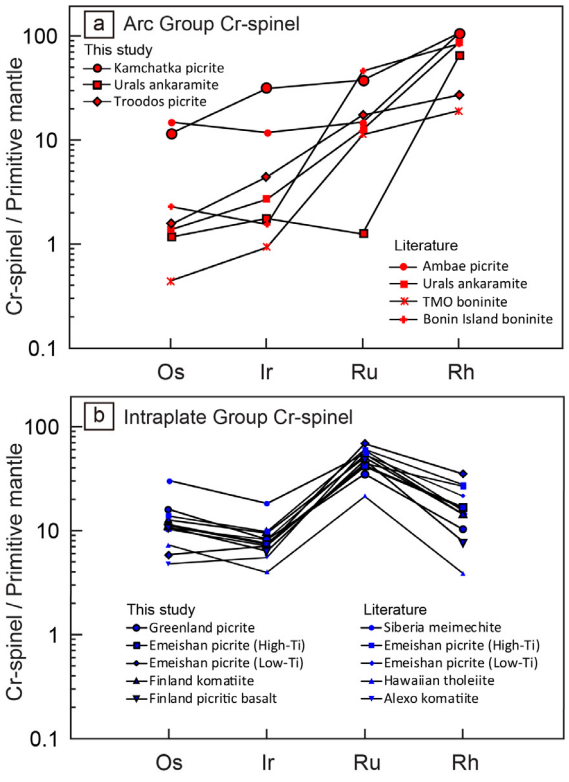

Fig. 4. Average Rh and IPGE contents of (a) Arc Group Cr-spinel and (b) Intraplate Group Cr-spinel from each locality normalized by primitive mantle values of McDonough and Sun (1995). Rh and IPGE contents of MORB Group Cr-spinel were not shown due to their low abundances. The compositions of Cr-spinels reported in literature are from Park et al. (2012), Kamenetsky et al. (2015) and Pagé and Barnes (2016).

Cr-spinels, but not for the Intraplate Group Cr-spinels (Fig. 7d). The Intraplate Group Cr-spinels are relatively enriched in Ru, Ir and Os and depleted in Rh compared to the Arc Group Cr-spinels at a given Fe^{3+}/R^{3+}. Iridium is positively correlated with Os (Fig. 8), whereas there is no clear correlation of Ir with Rh and Ru (not shown).

5. DISCUSSION

5.1. Trace elements in Cr-spinels

Although the major element chemistry of Cr-spinels has been widely used to constrain the petrogenesis and tectonic environments of their host volcanic rocks (e.g., Barnes and Roeder, 2001; Kamenetsky et al., 2001), there is shortage of trace element data for Cr-spinels. Pagé and Barnes (2009) have measured trace element compositions of Cr-spinels from boninites of the Thetford Mines Ophiolite and Bonin Island, and MORB from the EPR. They found discernible differences between Cr-spinels from boninite and MORB. Recently, Park et al. (2012) and Kamenetsky et al. (2015) have measured trace elements in Cr-spinel from the Ambae picrite, Siberia meimechite and Urals ankaramite. Our results, together with the data from previous studies, show that there are systematic differences in trace element abundances and ratios for Cr-spinel from the various magma types. In Fig. 2, the Arc Group Cr-spinels are characterized by fractionated patterns with enrichment of Sc, Mn and Co and depletion of Ni relative to the EPR MORB Cr-spinels (Pagé and Barnes, 2009). Vanadium shows the largest variation in the Arc Group Cr-spinels. The Cr-spinels from relatively reduced boninite contain systematically more V than those from oxidized island arc picrites with high Fe^{3+}/R^{3+} (Fig. 2a). The V contents of Cr-spinels decrease with increasing Fe^{3+}/R^{3+} in Fig. 7e. This variation is largely due to multivalent state of V in natural magmatic system (V^{2+}, V^{3+}, V^{4+} and V^{5+}; Sutton et al., 2005). Because vanadium can replaces trivalent or tetravalent cations in octahedral sites of Cr-spinels (Bordage et al., 2011) its partition coefficient decreases with increasing oxygen fugacity as V is oxidised to V^{5+}. Mallmann and O'Neill (2009) showed experimentally that the $D_V^{\text{Cr-spinel-silicate melt}}$ decreases from ~10 at QFM-1 to <1 at QFM + 2.

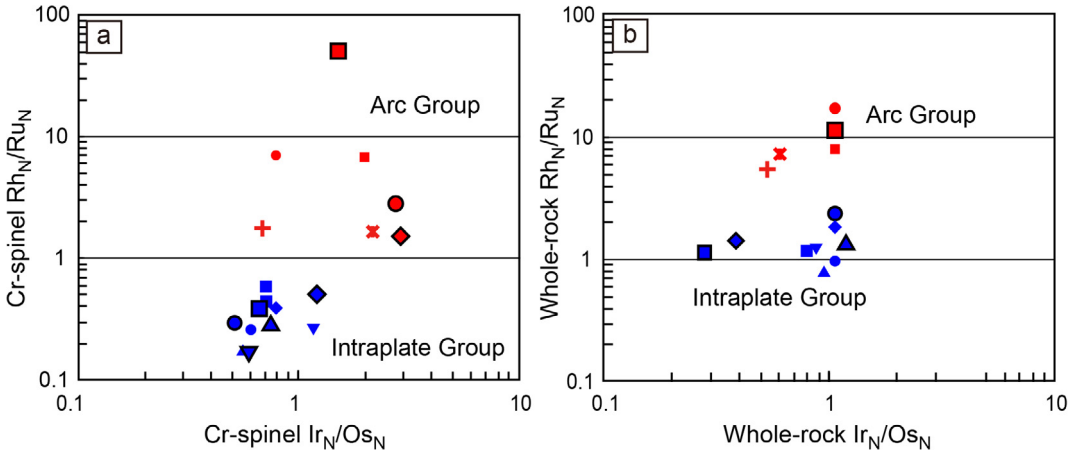

Fig. 5. Binary plots of Rh_N/Ru_N vs. Ir_N/Os_N ratios for (a) Cr-spinels and (b) host volcanic rocks. Note that the Arc Group Cr-spinels and host rocks are characterized by high Rh_N/Ru_N relative to those of the Intraplate Group at similar ranges of Ir_N/Os_N. Primitive mantle values for normalization are from McDonough and Sun (1995). For symbols see Fig. 1. The Rh and IPGE compositions of Cr-spinel and volcanic rocks reported in literature are from Park et al. (2012), Kamenetsky et al. (2015) and Pagé and Barnes (2016). The whole-rock compositions for the Urals ankaramite (Pe1023) are from this study.

Despite the large major element compositional variations in Cr-spinel phenocrysts (Fig. 1) and their parental melt, the Intraplate Group Cr-spinels exhibit similar trace element patterns (Fig. 2b). They are also characterized by slightly higher Sc, Mn, Co and Zn, and lower V and Ni than those from EPR MORB (Pagé and Barnes, 2009) as also shown in the Arc Group Cr-spinels. However, they can be distinguished from the Arc Group Cr-spinels by their high Ni and Ti contents (Fig. 2b). The Cr-spinels from Mid-Atlantic Ridge at 43°N, FAMOUS area, and Macquarie Island, analysed for this study, are depleted in Ni and Zn relative to the EPR MORB Cr-spinel (Pagé and Barnes, 2009). This can be partly attribute to the high Ni contents (565 ppm) in the MORB sample from the Garrett Transform Fault of EPR used by Pagé and Barnes (2009) whereas the MORB samples studied in this study contain 145–225 ppm Ni (Shibata et al., 1979; Kamenetsky and Eggins, 2012). However, it should be noted that the EPR MORB Cr-spinels contain 1766 ppm Ni (Pagé and Barnes, 2009), which is the highest Ni contents among all measured Cr-spinels (Fig. 7f). Given that intraplate magmas are commonly more enriched in Ni than MORB magmas (Niu et al., 2011), it requires other factors to explain the extremely high Ni contents in the EPR MORB Cr-spinels reported by Pagé and Barnes (2009).

The trace element data of Cr-spinels can be used to constrain the composition of the magma from which they crystallized and hence their tectonic setting and provide complementary information to that obtained from the major elements. Our study shows that Arc Group Cr-spinels show the highly fractionated trace element patterns with enrichment of Sc, Mn and Co and depletion of V compared to the MORB Group Cr-spinels (Fig. 2), which agrees with Pagé and Barnes (2009). The discrepancy between the two groups are particularly important in understanding petrogenesis of mantle podiform chromitites because most of them form either at arc or mid-ocean-ridge settings.

5.2. Enrichment of Rh and IPGEs in Cr-spinel

Our results show that Cr-spinels from diverse tectonic settings are variably enriched in Rh and IPGEs compared to the melts from which they crystallized. This confirms the conclusions of previous studies, based on *in situ* analysis of natural Cr-spinel (Locmelis et al., 2011; Park et al., 2012; Pagé et al., 2012; Kamenetsky et al., 2015; Pagé and Barnes, 2016; Arguin et al., 2016) and experimental study of Brenan et al. (2012) that Cr-spinel can be an important host for Rh and IPGEs in solid solution. The constant counts rate of Rh and IPGEs in the LA-ICP-MS time-resolved spectra (Fig. 3), and the correlations of Rh and IPGE contents with Cr-spinel compositional parameters, such as Fe^{3+}/R^{3+} (Fig. 7), show that these elements are held in the Cr-spinel lattice and not in inclusions. Homogeneous distribution of sub-micron-sized PGE-clusters in Cr-spinel may produce similarly constant count rates during ablation, but this option is highly unlikely, as discussed in detail by Pagé and Barnes (2016). They excluded this possibility with the argument that if there were PGE clusters, the size of such inclusions should be from >0.15 to 1.5 μm and hence they could be easily detected by backscattered electron image analysis and Pd and Pt should also be detected along with the other PGEs.

5.2.1. PGE contents in melts

The Rh and IPGE contents in Cr-spinels are controlled by the composition of the melts from which they crystallized and by the partition coefficients for these elements between Cr-spinels and silicate melts. Fig. 9 shows PM-normalized Rh and IPGE patterns for host volcanic rocks. The intraplate magmas have high Rh and IPGE contents, which are only slightly lower than those of primitive mantle values, and flat PM-normalized PGE patterns whereas arc magmas are characterized by fractionated patterns with relative enrichment of Rh and depletion of IPGEs. Flat PGE patterns are of typical intraplate magmas (Barnes et al.,

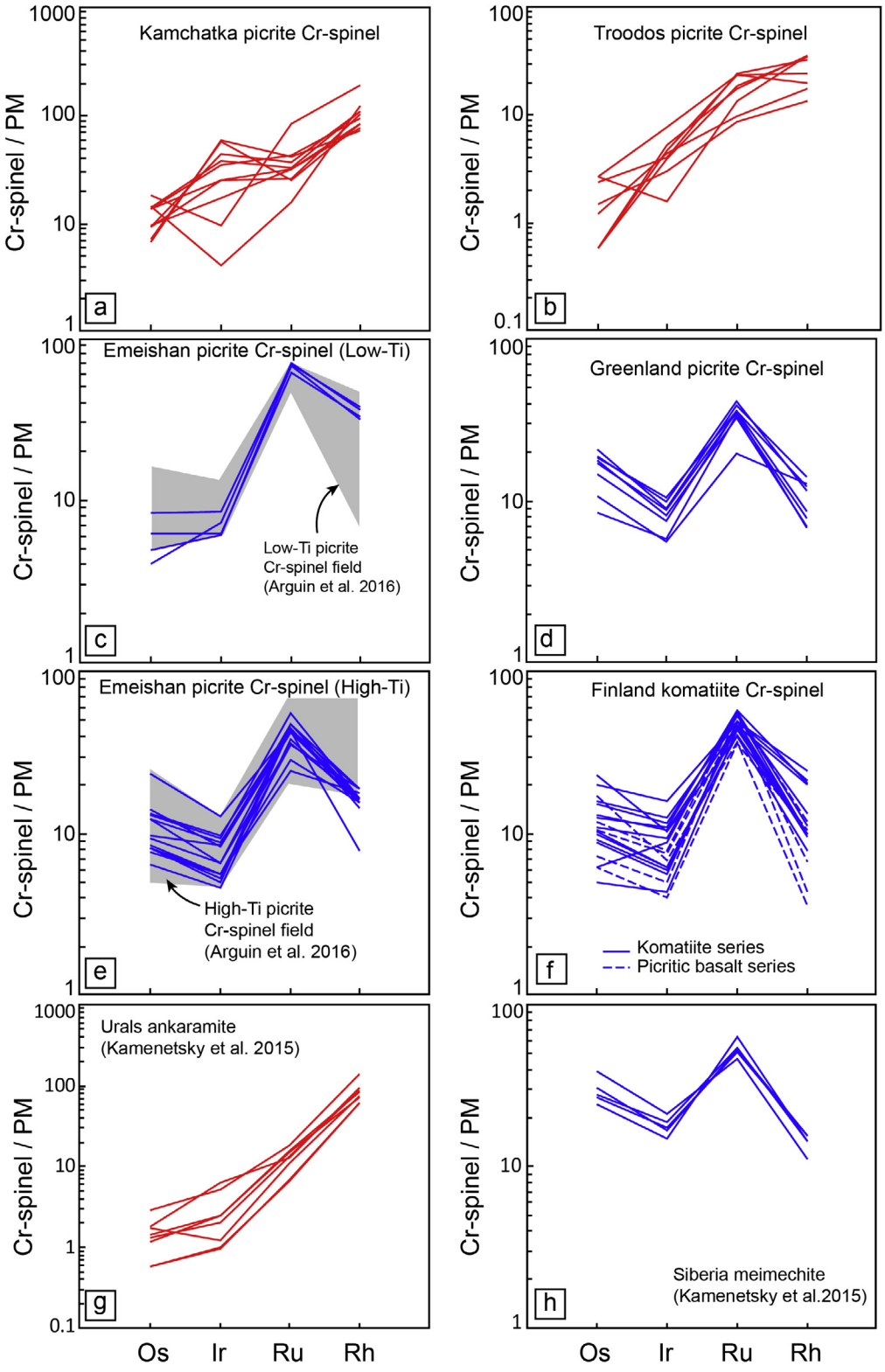

Fig. 6. Primitive mantle normalized Rh and IPGE contents of Cr-spinel from (a) the Kamchatka picrite, (b) the Troodos picrite, (c) the Emeishan low-Ti picrite (d) the Greenland picrite, (e) the Emeishan high-Ti picrite, (f) the Finland komatiite and picritic basalt, (g) Urals ankaramite and (h) Siberia meimechite. The gray fields in (c) and (e) are the compositions of Cr-spinel from the Emeishan low and high-Ti picrite previously reported in Arguin et al. (2016). The Urals and Siberia meimechite Cr-spinels compositions are from Kamenetsky et al. (2015).

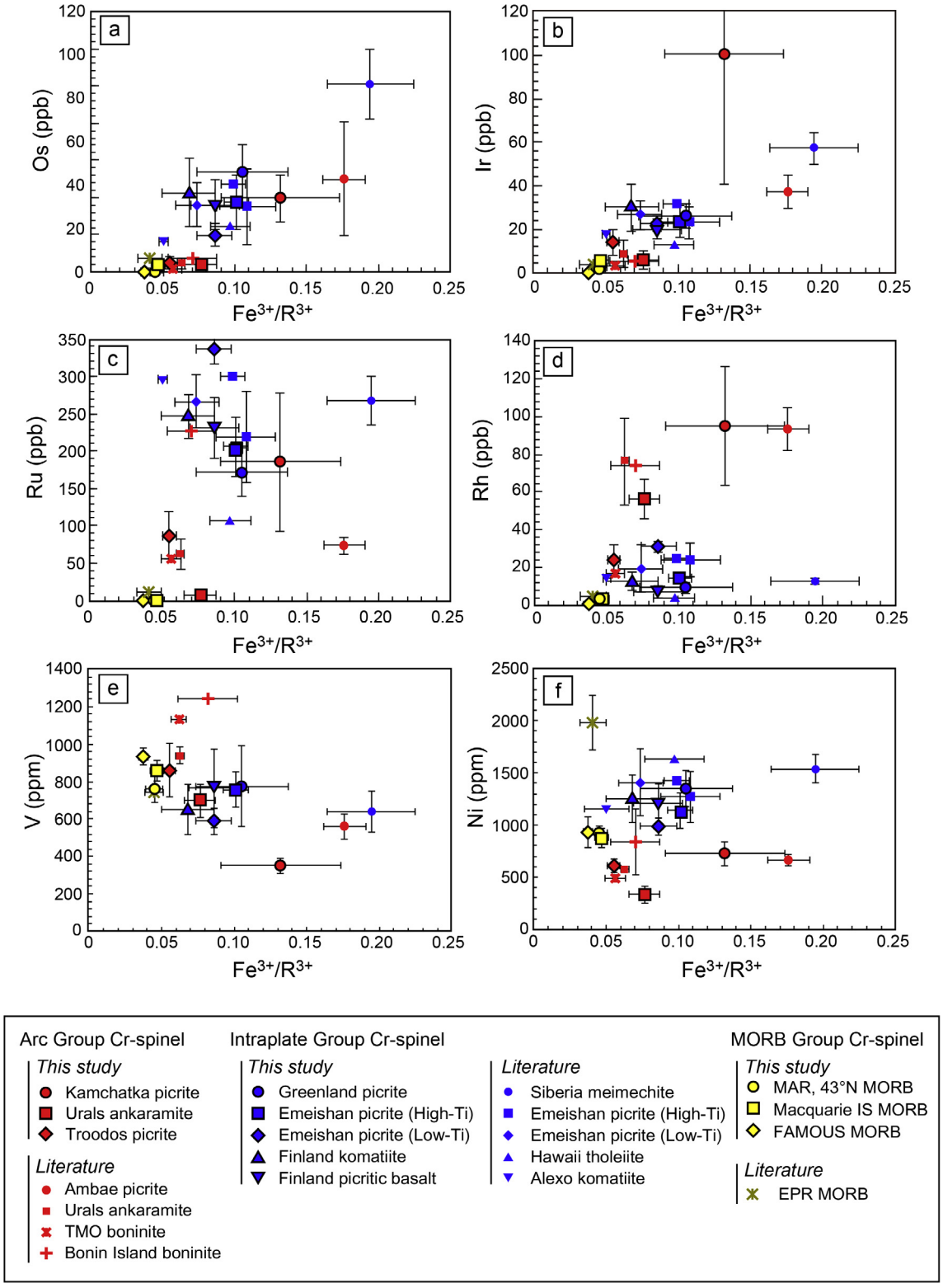

Fig. 7. Binary plots of Fe^{3+}/R^{3+} vs. (a) Os, (b) Ir, (c) Ru, (d) Rh, (e) V and (f) Ni. The error bars are one standard deviation of multiple analyses for Cr-spinel from each locality.

2015). The fractionated patterns of the Arc Group Cr-spinels and the overall flat patterns with positive Ru anomalies of the Intraplate Group Cr-spinels are inherited from their magma compositions (Figs. 4 and 9). This is also consistent with similar trends for both Cr-spinel and whole rock in a binary diagram of Rh_N/Ru_N vs Ir_N/Os_N (Fig. 5).

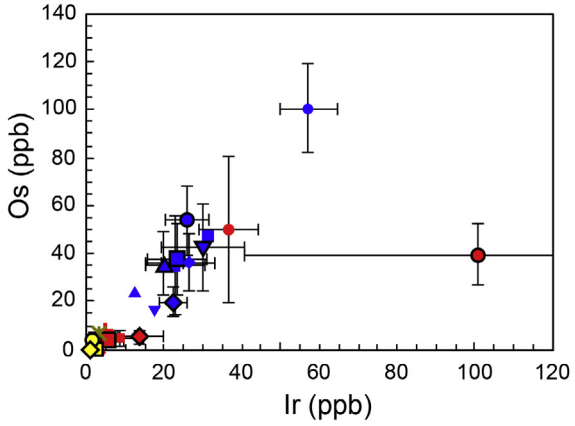

Fig. 8. Inter-correlation between Ir and Os in Cr-spinel. The error bars are one standard deviation of multiple analyses for Cr-spinels from each locality. Symbols as in Fig. 1.

These systematic differences between the Arc and Intraplate Group Cr-spinels have already been discussed by Park et al. (2015a) and Pagé and Barnes (2016) using fewer samples. The zigzag PGE patterns of the Intraplate Group Cr-spinels (Fig. 4b) and their low Rh_N/Ru_N, which are systematically below the whole-rock values (Fig. 5), suggest that there is also fractionation of Ru from Rh and other IPGEs due to differences in their compatibility in Cr-spinel.

The significantly lower PGE contents in MORB Group Cr-spinels results from the low abundances of Rh and IPGEs in MORB melts (Fig. 9c). The presence of sulphide blebs and compatible behaviour of PGEs in primitive MORBs from the MAR (Peach et al., 1990; Kamenetsky et al., 2013; Lissner et al., 2014) and Southwest Indian Ridge (Yang et al., 2014) suggest that Cr-spinel crystallized under sulfide-saturated conditions in primitive MORB melts from the two areas. Extraction of the sulfide melts will significantly deplete the coexisting MORB melts in all PGEs. Pagé and Barnes (2016) also attributed the low PGE contents in the MORB Group spinels to sulfide saturation during MORB magma generation. In contrast the high Rh and IPGE contents of the Arc and Intraplate Group Cr-spinels analysed in this study suggests that they crystallized from sulfide-undersaturated magmas.

5.2.2. PGM crystallization

There is a growing evidence for co-crystallization of PGMs with Cr-spinel (Brenan and Andrews, 2001; Barnes and Fiorentini, 2008; Park et al., 2012, 2013; Kamenetsky et al., 2015; Arguin et al., 2016). Because these PGMs include phases with different PGE affinities (e.g. Ru-rich laurite, Ir-rich or Pt-rich alloys), fractional crystallization of these phases will change the PGE contents in melts by fractionating one element with respect to others, and hence the PGE contents in Cr-spinels. The Cr-spinels analysed in this study show sub-parallel Rh and IPGE patterns within a given suite, except for those from the Kamchatka picrite (Fig. 6). This suggests that it is unlikely that the melts were saturated with IPGE and Rh bearing alloy or sulfide phases during fractionation of the primitive Cr-spinels from the

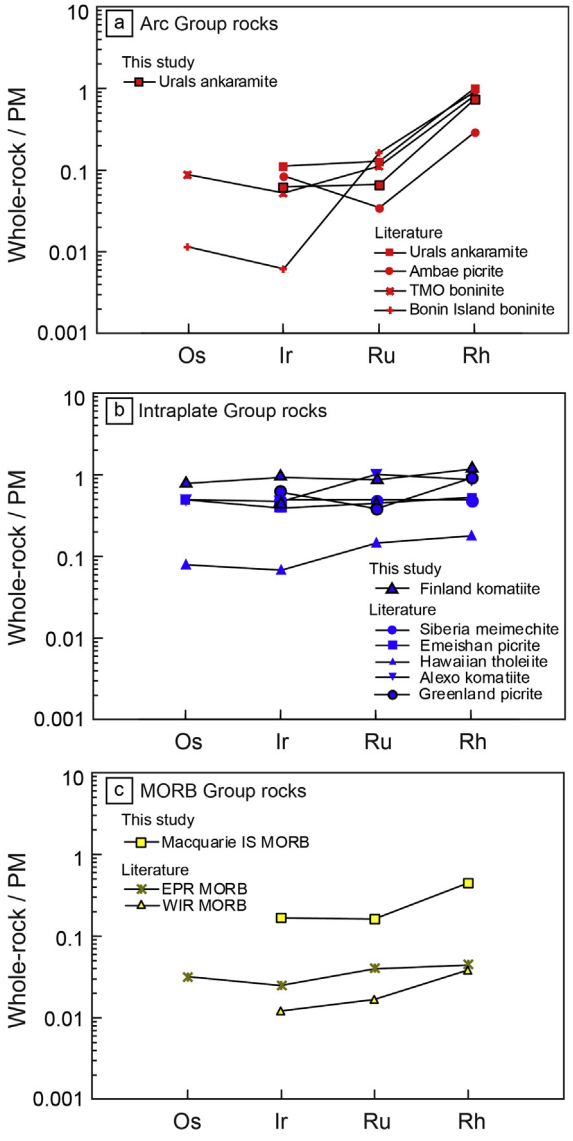

Fig. 9. Primitive mantle normalized Rh and IPGE contents in (a) Arc Group, (b) Intraplate Group and (c) MORB Group host volcanic rocks. Primitive mantle values used for normalization are from McDonough and Sun (1995). Literature whole-rock Rh and IPGE compositions are from Philipp et al. (2001), Li et al. (2012), Park et al. (2012), Pagé and Barnes (2016) and Yang et al. (2014).

Greenland picrite, Finland komatiite and picritic basalts, and Emeishan picrites. The spikes in the time-resolved spectra of LA-ICP-MS analysis (Fig. 3b; Appendix B) indicate formation and entrapment of PGE-rich phases by local reduction near the rim of growing Cr-spinel grains (e.g. Finnigan et al., 2008), but there is no evidence that this has had a detectable influence on the PGE geochemistry of the spinels. However, Rh and IPGE patterns of the Kamchatka Cr-spinels show marked variations especially in Ir (Fig. 6a). Also, $Pt \pm Ir \pm Os$ spikes were observed more frequently in the Cr-spinels from the Kamchatka picrite (4 out of 10 analyses) than in Cr-spinels from other locations. These observations suggest that the Kamchatka

magma was saturated with an Ir-bearing Pt-alloy during Cr-spinel crystallization, which preferentially depleted the melt in Ir relative to other IPGEs, leading to the Ir depletion in some Cr-spinels. The similar phenomenon was also observed in the Cr-spinels from the Ambae picrite, Vanuatu arc (Park et al., 2012).

5.2.3. Magnetite components of Cr-spinel

Brenan et al. (2012) have shown experimentally that the partitioning of Rh and IPGEs between Cr-spinel and silicate-melt is largely controlled by Fe^{3+} contents (i.e. magnetite component) in Cr-spinel due mainly to the high octahedral site preference energy of these elements. Rhodium and Ir are mostly divalent in natural magmatic systems (Borisov and Palme, 1995; Ertel et al., 1999) and have seven electrons in the outermost d shell in the low spin state (Zhang et al., 2010), suggesting a strong affinity for the octahedral site. Ruthenium is dominantly trivalent in magmas (Borisov and Nachtweyh, 1998) with five electrons in the outermost d shell in the low spin state (Geschwind and Remeika, 1962). The octahedral site preference energy is likely to be lower for Ru than Rh and Ir because Ru has zero tetrahedral crystal field stabilization energy (e.g., Burns and Fyfe, 1964).

Brenan et al. (2012) suggested that as Fe^{3+} content of Cr-spinel increases, more divalent octahedral sites become available in its lattice, which increases the partition coefficients of the divalent Rh and IPGEs. This suggestion is consistent with previous experimental studies on magnetite, which have yielded extremely high partition coefficients for Rh (up to 530), Ru (up to 1143) and Ir (up to 22,000) (Capobianco and Drake, 1990, 1994; Righter et al., 2004). Park et al. (2012) provided supporting evidence for this hypothesis using natural samples. They measured the Rh and IPGE contents of Cr-spinel from the highly oxidized Ambae picrite from Vanuatu ($fO_2 = QFM + 2.5$), and showed that Rh, Ru and Os correlate positively with the Fe^{3+}/R^{3+} ratio of Cr-spinel. However, these correlations were not clearly observed in the recent LA-ICP-MS study of natural Cr-spinel by Pagé and Barnes (2016) in which they compared Cr-spinel compositions from diverse magmatic systems. They suggested that the correlation between Fe^{3+} and Rh and IPGE in Cr-spinel could be due to the number of vacancies in the spinel because Fe^{3+} contents are calculated assuming perfect stoichiometry.

Our dataset, which covers a broader ranges of Fe^{3+}/R^{3+} than the previous studies, clearly shows that the Fe^{3+} content of Cr-spinel is the dominant factor for controlling the enrichment of Os, Ir and possibly Rh in Cr-spinel (Fig. 7). Iridium and Os are positively correlated with Fe^{3+}/R^{3+} in Cr-spinel in all samples although the Intraplate Group Cr-spinels contain systematically higher Ir and Os contents than those from the Arc Group Cr-spinels at a given Fe^{3+}/R^{3+} (Figs. 7a and b). This is partly due to the Intraplate Group magmas have an approximately one order of magnitude higher Ir and Os content (Fig. 9). For the Arc Group Cr-spinels a positive correlation between Rh and Fe^{3+}/R^{3+} exists, whereas the Intraplate Group Cr-spinels do not show any correlation. However, such correlations are observed within some individual volcanic suites such as the Greenland picrite (this study), Siberia meimechite (Kamenetsky et al., 2015) and Emeishan picrite (Arguin et al., 2016). The scattered Rh trends for the Intraplate Group Cr-spinels, from different localities, are probably because of their concentrations being close to the detection limits of the LA-ICP-MS (<1–5 ppb).

Ruthenium behaves differently from the other IPGEs and is not correlated with Fe^{3+}/R^{3+}, indicating that the availability of the divalent octahedral site is not a critical factor controlling the Ru partitioning to Cr-spinel. These trends are consistent with the different valence states of Rh and IPGEs. Rhodium and Ir are usually divalent in natural magmas (Borisov and Palme, 1995; Ertel et al., 1999), so that their partition coefficients are thought to increase as the number of divalent octahedral sites in the Cr-spinel increases, whereas Ru can be both divalent and trivalent (Borisov and Nachtweyh, 1998). As a consequence, the partitioning of Ru is more complex due to combined effects of Ru^{2+} and Ru^{3+} substitution. Having similar ionic radius and the same charge, divalent Ru should behave similarly to divalent Ir and Rh and partition strongly into Cr-spinels with a high magnetite component. In contrast, the partition coefficient for trivalent Ru will not be significantly influenced by increasing magnetite components in Cr-spinel because of abundant trivalent octahedral sites in Cr-spinel. The relatively higher Ru content of the Intraplate Group Cr-spinels compared with the Arc Group Cr-spinels, at a given Fe^{3+}/R^{3+}, suggests that the magma composition is the principal controlling factor (Fig. 7c).

The valence state of Os is poorly constrained compared to other PGEs mainly because it is highly volatile under oxidized conditions and has a low solubility in silicate melts, which makes it difficult to investigate experimentally. Fortenfant et al. (2006) attempted solubility experiments under highly oxidized conditions at $fO_2 > QFM + 2$ and 1350 °C and suggested that Os is trivalent under these conditions. However, the positive correlations with the Ir and magnetite components of the Cr-spinel (Figs. 7a and 8) in this study clearly show that Os behaves like other divalent cations and partitions in Cr-spinel as Os^{2+}. This suggests that the valency of Os is 2 + even under the oxygen fugacity conditions of natural magmatic systems analysed in this study ($\sim$QFM-1 < fO_2 < QFM + 2.5) or that the previously determined valence state was too high. The estimation of the valence state by Fortenfant et al. (2006) was based on 3 data points. Further experimental studies are required to confirm their conclusions.

5.3. Empirical partition coefficients between Cr-spinel and silicate melt

Mass balance studies, using the PGE content of volcanic Cr-spinels and their host rocks, have shown that Cr-spinel may account for a large fraction of the whole-rock PGE budget (up to 40% for Os, 25% for Ir, 30% for Rh, and 30–100% for Ru; Pagé and Barnes, 2016). Therefore, one should be cautious about using PGE contents of the host rocks as a proxy for melt compositions. Park et al. (2012) used the PGE content of an aphyric picritic lava and the compositions of Cr-spinel in equilibrium with the lava to

estimate Cr-spinel-silicate melt partition coefficients. Arguin et al. (2016) used the composition of a primitive melt after correcting the influence of Cr-spinel and olivine accumulation on whole-rock PGE contents (Li et al., 2012). Instead, Pagé and Barnes (2016) used PGE contents of the volcanic rocks as estimates of melt compositions. Because the role of silicate minerals in the whole-rock PGE budget is not understood, they argued that corrections for the effect of silicate minerals may not be straightforward and can introduce another source of error. If we assume that the PGEs do not partition into the silicate minerals ($D = 0$), accumulation of the silicate phenocrysts will dilute the melt composition. However, recent experimental studies on the PGE partitioning between olivine and silicate melt have shown that these elements can be moderately compatible in olivine ($D_{Rh,\ Ru,\ Ir}^{olivine\text{-}silicate\ melt} = 0.5–2.7$; Brenan et al., 2003, 2005).

In this study, we estimate the empirical Ds for the partitioning of Rh and IPGE between Cr-spinel and silicate melt using the concentrations of these elements in Cr-spinels and their host volcanic rocks where available, or similar rocks from the same volcanic series if the host rock is not available, after deducting the Rh and IPGEs held in the Cr-spinel from the whole-rock. We used the mass balance method suggested by Pagé and Barnes (2016) as reported in Appendix A.

For the Urals ankaramite the host volcanic rock (Pe1023), and for the Macquarie Island MORB the most primitive volcanic glass (8.8 wt.% MgO; sample 47,979) in the same suite, were used for estimating the empirical partition coefficients (Table 1). The PGE contents of a komatiite sample 12C-PPR-97, which was collected from the same outcrop as 12D-PPR-97 (Table 1), were used as proxies for the melt compositions for both the Finland komatiite and picritic basalt samples. The Cr-spinels from the two suites show almost identical PGE patterns (Fig. 6f), suggesting similar PGE concentrations in both melts. Average PGE contents of the Greenland picrite ($n = 6$; 19–26 wt.% MgO; Philipp et al., 2001), Emeishan high-Ti ($n = 3$; 24–27 wt.% MgO and $TiO_2 > 1$ wt.%; Zhang et al., 2005; Li et al., 2012) and low Ti picrites ($n = 6$; 21–27 wt.% MgO and $TiO_2 < 1$ wt.%; Li et al., 2012) were used to calculate the empirical partition coefficients for spinels from these suites. The PGE contents of the Ambae aphyric picrite from the Vanuatu arc (10.7 wt.% MgO; Park et al., 2012) and the Thetford Mines Ophiolite boninite (Pagé and Barnes, 2016) were used for the Kamchatka arc picrite and the Troodos boninite samples, respectively. Mass balance calculations (Appendix B) show that the contribution from Cr-spinel to the whole-rock Rh, Ir and Os contents are less than 10% for most samples although 20–65% of the Ru contents in the whole-rock compositions can be accounted for by Cr-spinel in the Greenland picrite, the Finland komatiite and picritic basalt, the Siberia meimechite, and Emeishan picrite. The rest of the whole-rock PGE budget is held in the fine-grained matrix as well as in silicate mineral phenocrysts, sulfide and alloy phases. Therefore, the calculated empirical partition coefficients are the minimum values.

The empirical partition coefficients calculated using whole-rock PGE contents after subtracting the contributions from Cr-spinel microphenocrysts are reported Table 4. For all the samples Ru is the most compatible among PGEs with the partition coefficients ranging from 18 to 3708 (Table 4), which can be explained by it having the highest affinity for the trivalent octahedral site. Rhodium and other IPGEs show similar but, variable compatibilities with D values of 7–641. In order to quantitatively show the variations in the partition coefficients with the magnetite component, Brenan et al. (2012) has expressed the partition coefficients for divalent and trivalent cations as follows:

$$D^{2+}_{molar} = (k^{2+}_{tet}((1-x)/3)) + (k^{2+}_{oct}(x/3))$$

$$D^{3+}_{molar} = (k^{3+}_{tet}(x/3) + (k^{3+}_{oct}(2-x)/3))$$

where D^{2+}_{molar} and D^{3+}_{molar} are mineral/melt partition coefficients for divalent and trivalent cations (mole% ratio), respectively, k^{2+}_{tet} and k^{2+}_{oct} are divalent cation affinity for IV- and VI-coordinated sites respectively, k^{3+}_{tet} and k^{3+}_{oct} are trivalent cation affinity for IV- and VI-coordinated sites, respectively, and x is the spinel inversion parameter, which is the fraction of the inverted spinel components in which divalent cations occupy half of the octahedral sites. The parameter ranges from 0 for normal spinel (e.g. chromite) and 1 for fully inverted spinel (e.g. magnetite). The inversion parameter was calculated at 1300 °C following the method of Kurepin (2005). Brenan et al. (2012) modelled the variation in the PGE partitioning with the inversion parameter in a binary Fe_3O_4-$FeCr_2O_4$ system because the effects of $MgAl_2O_4$ and $FeAl_2O_4$ components are compensated by each other. The high temperature site occupancies are similar in the $MgAl_2O_4$-Fe_3O_4 systems (Mattioli and Wood, 1988) whereas the addition of $FeAl_2O_4$ reduces the amount of the divalent octahedral sites (Nell et al., 1989). Model 1 and 2 in Fig. 10 show the variations in partition coefficients for divalent and trivalent cations, respectively.

Fig. 10 shows the variations in the partition coefficients for Rh and IPGEs plotted against the inversion parameter, $Fe^{3+}/(Fe^{3+}+Cr^{3+})$, in the Fe_3O_4-$FeCr_2O_4$ system. The D values calculated in this study are consistent with previously reported experimental and empirical data and the modelled variations (Model 1 in Fig. 10) by Brenan et al. (2012). These confirm the validity of using whole-rock PGE contents in volcanic rocks after correcting the Cr-spinel effect as proxies for silicate melt compositions. The D values for Rh, Ir, and Os increase with increasing $Fe^{3+}/(Fe^{3+}+Cr^{3+})$ in Cr-spinel following the trends of Model 1, which suggests that these elements are mostly divalent in the magmatic systems and their partitioning is controlled by the availability of divalent octahedral sites in Cr-spinel.

Note that the Arc Group spinels have consistently higher D values for Rh and IPGEs at a given $Fe^{3+}/(Fe^{3+}+Cr^{3+})$ ratio than those from Intraplate Group (Fig. 10). The compositions of the Intraplate and MORB Group Cr-spinels, together with experimental results (Brenan et al., 2012), are best explained by Model 1 with the affinity of divalent Rh, Ir and Os for the VI-coordinated site (k^{2+}_{oct}) of

Table 4
Empirical partition coefficients of Rh and IPGE ($D^{Cr\text{-}spinel\text{-}silicatemelt}$).

Sample type	References	Cr-spinel compositions				Whole-rock compositions after subtracting Cr-spinel accumulation				Empirical parition coefficients $D^{Cr\text{-}spinel\text{-}silicatemelt}$			
		Ru (ppb)	Rh (ppb)	Os (ppb)	Ir (ppb)	Ru (ppb)	Rh (ppb)	Os (ppb)[a]	Ir (ppb)	D_{Ru}	D_{Rh}	D_{Os}[a]	D_{Ir}
Arc group													
Kamchatka picrite[b]	This study	185	95	40	101	0.05	0.15	*0.18*	0.18	3708	633	*219*	561
Urals ankaramite	This study	6	56	4	6	0.34	0.67	*0.20*	0.20	18	84	*20*	29
Troodos picrite[c]	This study	87	24	5	14	0.58	0.76	0.30	0.17	150	32	17	82
Ambae picrite	Park et al. (2012)									2448	641	280	472
Urals ankaramite	Kamenetsky et al. (2015)									105	89	14	26
Bonin Island boninite	Pagé and Barnes (2016)									284	86	193	243
TMO boninite	Pagé and Barnes (2016)									102	22	n.d.	17
Intraplate group													
Greenland picrite[d]	This study	172	9	54	26	1.41	0.81	*1.80*	1.90	122	11	*30*	14
Emeishan picrite (High-Ti)[e]	This study	206	15	38	23	1.10	0.38	5.57	1.40	186	38	7	17
Emeishan picrite (Low-Ti)[f]	This study	336	31	20	22	0.66	0.44	3.22	1.09	512	70	6	20
Finland komatiite	This study	246	13	43	30	2.46	0.98	2.42	2.84	100	13	18	11
Finland picritic basalt	This study	231	7	36	20	2.52	1.02	2.46	2.91	92	7	15	7
Siberia meimechite	Kamenetsky et al. (2015)									104	28	63	36
Emeishan basalts (High-Ti)	Arguin et al.(2016)									112	37	27	17
Emeishan basalts (Low-Ti)	Arguin et al.(2016)									136	30	27	20
Emeishan basalts	Pagé and Barnes (2016)									132	51	28	25
Hawaiian tholeiite	Pagé and Barnes (2016)									146	22	91	58
Alexo komatiite	Pagé and Barnes (2016)									56	18	10	12
MORB group													
Macquarie Island MORB	This study	<10	2.7	4.1	5.6	0.80	0.39	*0.53*	0.53	n.d.	7	*8*	11
EPR MORB	Pagé and Barnes (2016)	25	12	7.2	3.4	0.20	0.04	0.11	0.08	62	110	67	43

n.d., not determined.

[a] Os contents in italics are assumed to be the same as for Ir contents.

[b] Ambae arc aphyric picrite composition (Park et al., 2012) are used for whole-rock PGE contents.

[c] TMO (Thetford Mines Ophiolite) boninite compositions (Pagé and Barnes, 2016) are used for whole-rock PGE contents.

[d] Average Greenland picrite compositions (n = 6; 19–26 wt.% MgO; Philipp et al., 2001) are used for whole-rock PGE contents.

[e] Average Emeishan high-Ti picrite composition (n = 3; 24–27 wt.% MgO and TiO2 > 1 wt.%; Zhang et al. 2005 and Li et al. 2012) is used for whole-rock PGE contents.

[f] Average Emeishan high-Ti picrite composition (n = 6; 21–27 wt.% MgO and TiO2 < wt.%; Li et al. 2012) is used for whole-rock PGE contents.

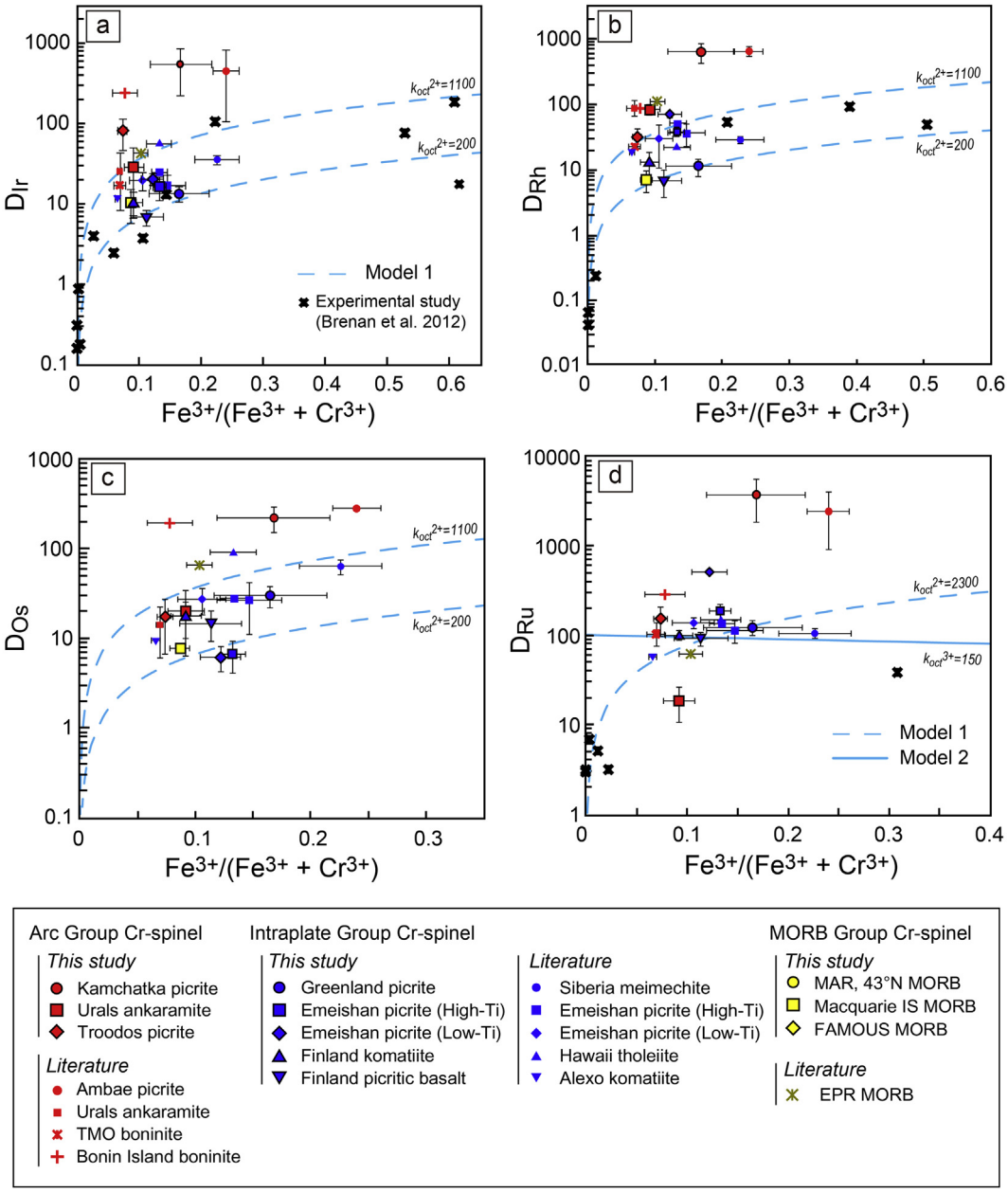

Fig. 10. Binary plots of $Fe^{3+}/(Fe^{3+} + Cr^{3+})$ vs. (a) D_{Ir}, (b) D_{Rh}, (c) D_{Os}, and (d) D_{Ru}. Model 1 represents variations in partition coefficients of divalent Rh and IPGEs against $Fe^{3+}/(Fe^{3+} + Cr^{3+})$ in Cr-spinel with different k_{oct}^{2+}. Model 2 shows variations in partition coefficients of trivalent Ru with $Fe^{3+}/(Fe^{3+} + Cr^{3+})$ in Cr-spinel. The error bars represent one standard deviation of multiple analyses for Cr-spinels from each locality.

200–1100 and for the IV-coordinated site (k_{tet}^{2+}) of 0.9 whereas a k_{oct}^{2+} of >6500 is required for the Arc Group Cr-spinels, which suggests that these elements are more compatible in Cr-spinel from arc magmatic systems at similar ranges of magnetite components (Fig. 10).

The variations in the *D* values for Ru are different from Rh and other IPGEs. Their partition coefficients are higher by a factor of ~10 compared to the *D* values for Rh, Ir, and Os at $Fe^{3+}/(Fe^{3+}+Cr^{3+})$<0.1, but they slightly decrease with increasing inversion parameter at $Fe^{3+}/(Fe^{3+}+Cr^{3+})$ of >0.1 (Fig. 10d). This trend may result from the multi-valence states of Ru in silicate melts. At relatively reducing conditions (i.e. lower inversion parameter), the amount of divalent Ru in silicate melts is high and its partitioning into Cr-spinel is dependent on the magnetite component, whereas under more oxidizing conditions (i.e. higher inversion parameter), the fraction of trivalent Ru increases and its D value will be less affected by magnetite components in the Cr-spinel. Fig. 10d shows two models for $D_{Ru}^{Cr\text{-spinel-silicate melt}}$ variations for the Intraplate Group Cr-spinels and for experimental results (Brenan et al., 2012) plotted against $Fe^{3+}/(Fe^{3+}+Cr^{3+})$ of the Cr-spinel.

Model 1 and 2 curves represent the trends of D values if the valence state of Ru is 2+ and 3+, respectively. Model 1 is consistent with the increasing trend at $Fe^{3+}/(Fe^{3+}+Cr^{3+}) < 0.1$, whereas Model 2 accounts for the slightly decreasing trend at $Fe^{3+}/(Fe^{3+}+Cr^{3+}) > 0.1$. The compositional variations of the Arc Group Cr-spinels require a high k_{oct}^{2+} of ~16,000 at k_{tet}^{2+} of 0.9.

At magmatic temperatures (>1000 °C), the $MgAl_2O_4$ component of the Cr-spinel can also have divalent octahedral (Mg) sites (Mattioli and Wood, 1988). However, its influence on Rh and IPGE partitioning may not be as dominant as magnetite because there is no correlation between Rh and IPGE contents and Al^{3+}/R^{3+} ($Al^{3+}/(Fe^{3+}+Cr^{3+}+Al^{3+})$) in Cr-spinel (Fig. 11). Rather, the maximum D values for Rh and IPGEs decrease with increasing Al^{3+}/R^{3+} due to decreasing Fe^{3+}/R^{3+}.

The estimated D values for the Arc Group Cr-spinels are consistently higher than those of the Intraplate Group Cr-spinels at the similar ranges of $Fe^{3+}/(Fe^{3+}+Cr^{3+})$ although the discrepancy becomes smaller at low $Fe^{3+}/(Fe^{3+}+Cr^{3+})$ (Fig. 10), which requires another factor to increase affinity of Rh and IPGE in the Arc Group Cr-spinel in addition to the magnetite components in Cr-spinels. These trends cannot be attributed to the differences in major element compositions of the Cr-spinel from each group because they have similar ranges of spinel parameters, such as Cr#, Mg# and Fe^{3+}/R^{3+} (Fig. 1). The TiO_2 contents of the Intraplate Group Cr-spinels are consistently higher than those of Arc Group Cr-spinels (Fig. 1a). However, the effect of ulvöspinel component would be the opposite to what is observed, because an increase in the fraction of the ulvöspinel component should increase the compatibility of divalent Rh and IPGEs in Cr-spinel.

One possible explanation is the temperature dependency of the divalent octahedral site in magnetite. Magnetite is a pure inverse spinel at room temperature, but the amount of ferrous iron in the octahedral site of the magnetite structure decreases with increasing temperature (Wißmann et al., 1998). The crystallization temperature of the Arc Group Cr-spinels is ~1200 °C (e.g. Ambae arc picrite; Eggins, 1993), which is generally 100 to 200 °C lower than those of the Intraplate Group Cr-spinels (~1300–1400 °C). Therefore, the Arc Group Cr-spinels have more divalent octahedral sites at the same level of the magnetite component, resulting in higher partition coefficients. This is consistent with the partition coefficients for the Intraplate Group Cr-spinels, which are comparable with those obtained by high-temperature experimental studies (1400 °C and 1900 °C; Brenan et al., 2012). However, the difference is less than a 10% reduction in the ferrous iron in the octahedral sites if the temperature is increased from 1200 to 1400 °C (Wißmann et al., 1998), and is not enough to explain the increase in D values by a factor of ~10 higher for the Kamchatka and the Ambae Cr-spinels compared with the Intraplate Group Cr-spinels at the same $Fe^{3+}/(Fe^{3+}+Cr^{3+})$.

5.4. Why do arc lavas have highly fractionated PGE patterns?

Several studies of the PGE geochemistry of arc lavas have shown that they are characteristically depleted in IPGEs relative to PPGEs (Woodland et al., 2002; Dale et al., 2012; Park et al., 2013, 2015b). The PM-normalized PGE patterns of arc basalts are compared with intraplate magmas such as the Hawaiian OIB and the Greenland CFB in Fig. 12. Arc basalts are enriched in Pd and significantly depleted in Ru and Ir, having Pd_N/Ir_N from 100 to 165 whereas the Hawaiian OIB and Greenland CFB are characterized by mildly fractionated patterns with Pd_N/Ir_N of 5–10 over a similar range of MgO contents. Our results show that these patterns can be explained by differences in the compatibility of Rh and IPGEs in Cr-spinel between arc magmas, OIBs and CFBs. The empirical partition coefficients of Rh and IPGE, with the exception of Ru are less than 91 for the Intraplate Group Cr-spinels (Table 4). Given an olivine/Cr-spinel ratio of 100:1 for most basaltic and picritic magmas (Roeder et al., 2006) and that the bulk D's for Rh and IPGEs are <1 in OIB and CFB magmas, Cr-spinel fractionation will have little influence

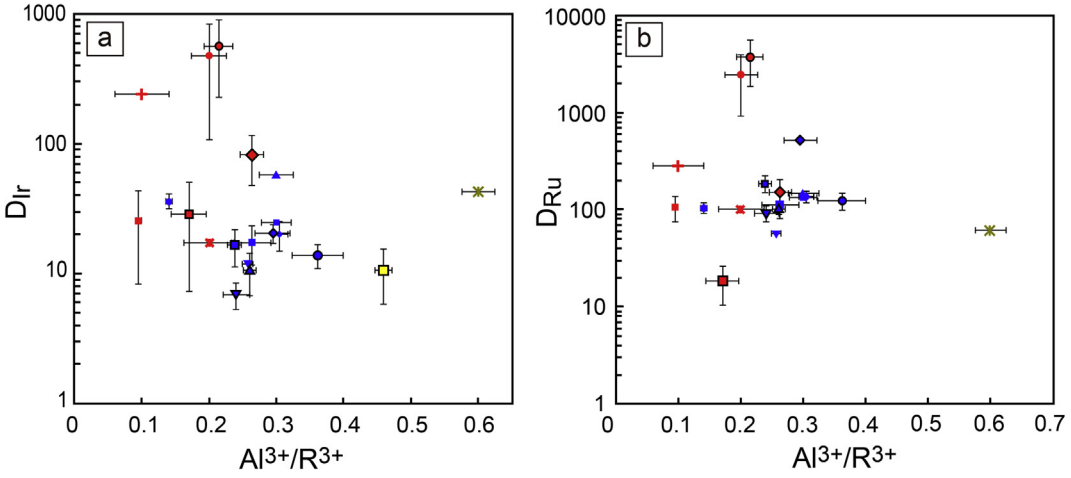

Fig. 11. Binary plots of Cr-spinel Al^{3+}/R^{3+} vs. (a) D_{Ir} and (b) D_{Ru}. Symbols as for Fig. 1.

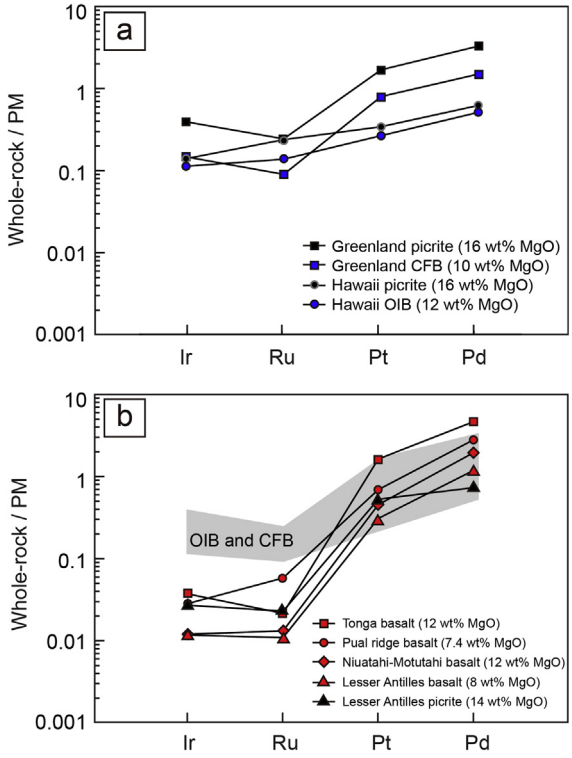

Fig. 12. Primitive mantle normalized PGE contents in basalts and picrites from various island arcs, Greenland and Hawaii. Primitive mantle values from McDonough and Sun (1995). Lesser Antilles picrite and basalt are an average of four picrites with 13.6–15.3 wt.% MgO and an average of three basalts with 5.8–10.5 wt.% MgO respectively from Woodland et al. (2002). Tonga central basalt is a weighted average of six analyses on two basalt samples with 10 and 14 wt.% MgO (Dale et al., 2012), Pual ridge basalt is an average values of four analyses on two samples with 7–7.8 wt.% MgO (Park et al., 2013). Niuatahi-Motutahi basalt is an average of three basalts with 7.2–14.3 wt.% MgO (Park et al., 2015b). Greenland picrite and basalt are an average of six picrite samples (14.2–19.1 wt.% MgO; Philipp et al., 2001) and twenty-one basalt samples (7.2–13.0 wt.% MgO; Philipp et al., 2001) respectively. Hawaii picrite and basalt are an average of seven picrites with 14.9–18.0 wt.% MgO and of six basalts from the Mauna Kea and Hualalai respectively (Ireland et al., 2009).

on Pd_N/Ir_N. This is consistent with the almost identical Pd_N/Ir_N of both picrites and basalts in Greenland and Hawaii (Fig. 12a). In contrast, the compatibilities of Rh and IPGEs in Cr-spinel are much higher in arc magmas, particularly under oxidized conditions ($D_{Rh\ and\ IPGE} > 200$ in the Ambae and Kamchatka Cr-spinel; Table 4). As a consequence, the role of Cr-spinel on fractionation of Pd from Ir is important in arc magmas, and Pd_N/Ir_N increases during magma differentiation (e.g., Dale et al., 2012; Park et al., 2013). The Pd_N/Ir_N increases from 27 to 103 during evolution of the Lesser Antilles arc picrite to basalts (Fig. 12b).

However, primitive arc picrites with >14 wt.% MgO are still more fractionated (Fig. 12b; $Pd_N/Ir_N = 27$ in Lesser Antilles picrites; Woodland et al., 2002) than picrites in association with OIBs and CFBs (Fig. 12a; $Pd_N/Ir_N < 10$) at similar MgO contents. This indicates that the fractionated patterns of arc basalts are partly inherited from their mantle sources or induced during partial melting. Dale et al. (2012) discussed the possible processes that can produce the highly fractionated PGE patterns in arc magmas. They attributed PPGE/IPGE fractionation to a large degree melting (~25%) of depleted harzburgitic mantle under oxidized conditions with residual IPGE-bearing alloys and Cr-spinel in the supra-subduction zone. During this process, sulfides would be completely consumed and thus contribute to the melt enrichment in Pd and Pt, although residual alloys and Cr-spinel would retain Rh and IPGEs in the mantle (Dale et al., 2012). The higher compatibility of Rh and IPGEs in the Arc Cr-spinel, particularly under oxidized conditions, as confirmed in this study, suggests that the Arc Cr-spinel has a strong influence on PGE fractionation during partial melting. *In situ* measurements of Rh and IPGEs in sub-arc mantle Cr-spinel should be performed to constrain the role of the residual mantle Cr-spinel quantitatively because Cr-spinels in the sub-arc mantle peridotite can be depleted in Fe^{3+} compared to arc volcanic Cr-spinels (e.g. Parkinson and Pearce, 1998) and can be in equilibrium with residual PGMs (Kepezhinskas et al., 2002).

We further suggest that formation of ophiolitic chromitite may fractionate PPGEs from IPGEs, also mentioned by Dale et al. (2012). Mantle chromitite is formed by interaction between ascending mantle-derived melts and ambient mantle at the crust-mantle boundary (Zhou et al., 1994; Arai, 1997). It has been suggested that moderately depleted harzburgitic mantle, compared with typical oceanic lithospheric mantle, facilitates Cr-spinel crystallization to form chromitite (Zhou et al., 1994; Arai, 1997). In contrast, reaction between lherzolitic mantle and high-Al MORB melts forms Al-rich chromitite (Arai, 1997). The upper mantle beneath arcs is considered to be mildly depleted and therefore favours Cr-rich chromitite formation, which is consistent with the observations that most of the large chromitite deposits occur in ophiolites produced at subduction zones (Dilek and Furnes, 2011). Furthermore, based on the result of this study, partitioning of Rh and IPGEs to Cr-spinel should be efficient in oxidized sub-arc mantle. This accounts for the relatively high abundances of Rh and IPGEs in Cr-rich chromitite formed in subduction zone compared with MOR-type Al-rich chromitite (Gonzalez-Jimenez et al., 2014 and references therein). However, it should be noted that Cr-spinels from ophiolitic mantle chromitites are depleted in Rh and IPGE (Pagé and Barnes, 2016) and contain IPGE-rich minerals as inclusions (e.g. Page et al., 1984; Prichard et al., 2017). It is still open to debate as to whether these IPGE-rich minerals co-crystallized with Cr-spinels and entrapped as inclusions, whether they formed by exsolution from Cr-spinels or whether they formed by diffusion towards base metal sulfide inclusions, as suggested by Pagé and Barnes (2016) and Barnes et al. (2016), during slow cooling. In any case the retention of Rh and IPGEs at depth is more likely in sub-arc mantle where Cr-rich chromitite forms (Dilek and Furnes, 2011), which can fractionate PPGE from IPGE in primitive arc magmas.

6. CONCLUSIONS

The trace element and PGE contents in Cr-spinel were measured from various magma types by the *in situ* LA-ICP-MS technique. Systematic differences were observed in trace element and PGE compositions between Cr-spinels from arc, intraplate and MORB magmas. The Arc Group Cr-spinels are enriched in Sc, Mn, and Co and depleted in Ni compared to the MORB Group Cr-spinels. The Intraplate Group Cr-spinels can be distinguished from Arc Group Cr-spinels by their high Ni contents.

Most of the studied Cr-spinels contain tens of ppb Rh and IPGEs in solid solution, except for Cr-spinel from MORB. The Arc Group Cr-spinels show characteristically fractionated PM-normalized PGE patterns with high Rh and low Ir contents. The Intraplate Group Cr-spinels have flat PGE patterns with positive Ru anomalies. The MORB Group Cr-spinels are PGE-poor. The trace element and PGE compositions of Cr-spinels, which reflect the magma compositions and conditions, can be used in conjunction with major element compositions, to constrain tectonic environments.

The enrichment of Rh and IPGEs in Cr-spinel is mainly controlled by the Rh and IPGE contents in silicate melts and the inverse spinel parameter, Fe^{3+}/R^{3+} (i.e. oxygen fugacity). The available evidence suggests that the influence of co-crystallizing PGM is negligible, as also shown in Pagé and Barnes (2016). The positive correlation between Rh, Ir, and Os contents and the magnetite component in Cr-spinel confirms the previous suggestion drawn from the experimental study of Brenan et al. (2012). Empirical partition coefficients for Rh and IPGE, calculated in this study increase with the inverse spinel parameter and agree well with the previously reported D values from experimental and empirical studies. However, the Arc Group Cr-spinels have systematically higher D values than those of the Intraplate Group Cr-spinels at a given Fe^{3+}/R^{3+}. Such discrepancy is partly due to lower temperature of the arc magmas than those of intraplate magmas, which causes increase in divalent octahedral site in Cr-spinel at the same magnetite fraction.

Due to the higher compatibility of Rh and IPGEs in Cr-spinel from arc magmas, compared with those from other tectonic settings, Cr-spinel inducted fractionation of the PGEs will be greatest in oxidized arc environments. The highly fractionated PGE patterns of arc primitive magmas can be explained by fractional crystallization of Cr-spinel in the early stage of magma differentiation, although some of the observed fractionation arises from mantle processes such as melting of depleted mantle with residual IPGE alloys and precipitation of chromitite as the ascending magma reacts with depleted harzburgite.

ACKNOWLEDGEMENTS

We thank Dr. Stephen Barnes and Dr. Philippe Pagé for their careful and constructive reviews, which helped to improve this paper. The guest editor, Dr. Chris Dale is thanked for through review, helpful suggestions and editorial handling. We thank Jihyuk Kim for proof reading. This study was funded by the Korea government Ministry of Science, ICT and Future Planning (NRF-2015R1C1A1A01054101) to J.-W. Park. The Russian Science Foundation (Grant #16-17-10145) provided funding to V. Kamenetsky. E. Hanski acknowledges support from Academy of Finland Grant #281859. The mineralogy and geochemistry of the Urals ankaramite was supported by RFBR Grant N 16-05-00508 to E. Pushkarev.

APPENDIX A. MASS BALANCE CALCULATION AND ESTIMATION OF EMPIRICAL PARTITION COEFFICIENTS $D_{METAL}^{CR\text{-}SPINEL\text{-}SILICATE\ MELT}$

The mass balance calculation was performed using the method described in Pagé and Barnes (2016). The mass fraction of Cr-spinel in a volcanic rock (%Cr-spinel) was estimated with the following equation:

$$\%\ \text{Cr-spinel} = Cr_2O_3^{WR}/Cr_2O_3^{Cr\text{-spinel}} \times 100 \times 0.75$$

where $Cr_2O_3^{WR}$ = whole-rock Cr_2O_3 content and $Cr_2O_3^{Cr\text{-spinel}} = Cr_2O_3$ contents in Cr-spinel. This calculation assumes that 75% of Cr from the whole-rock is hosted by Cr-spinel, as suggested by Arguin et al. (2016). The mass fraction of Cr-spinel is used to estimate the proportion of contribution from Cr-spinel in the whole-rock PGE budget expressed as follows:

$$F_i^{\text{Cr-spinel}}\ (\%) = 100 \times (C_i^{\text{Cr-spinel}} \times \%\text{Cr-spinel})/C_i^{WR}$$

where $F_i^{\text{Cr-spinel}}(\%) = \%$ of contribution from Cr-spinel in the whole-rock for element i, $C_i^{\text{Cr-spinel}}$ = Content of element i in Cr-spinel, and C_i^{WR} = Content of element i in the whole-rock. To constrain the empirical partition coefficient, we estimated the PGE contents in silicate melts with the following equation:

$$\begin{aligned} C_i^{\text{melt}} &= \text{Content of element } i \text{ in silicate-melt} \\ &= (C_i^{WR} \times 100 - C_i^{\text{Cr-spinel}} \times \%\text{Cr-spinel})/(100 \\ &\quad - \%\text{Cr-spinel}). \end{aligned}$$

APPENDIX B. SUPPLEMENTARY MATERIAL

Supplementary data associated with this article can be found, in the online version, at http://dx.doi.org/10.1016/j.gca.2017.05.039.

REFERENCES

Arai S. (1997) Origin of podiform chromitites. *J. Asian Earth Sci.* **15**, 303–310.

Arguin J.-P., Pagé P., Barnes S.-J., Yu S.-Y. and Song X.-Y. (2016) The effect of chromite crystallization on the distribution of osmium, iridium, ruthenium and rhodium in picritic magmas: an example from the Emeishan Large Igneous Province, Southwestern China. *J. Petrol.* **57**, 1019–1047.

Ballhaus C. and Sylvester P. (2000) Noble metal enrichment processes in the Merensky Reef, Bushveld Complex. *J. Petrol.* **41**, 545–561.

Barnes S.-J., Naldrett A. J. and Gorton M. P. (1985) The origin of the fractionation of platinum-group elements in terrestrial magmas. *Chem. Geol.* **53**, 303–323.

Barnes S. J. and Fiorentini M. L. (2008) Iridium, ruthenium and rhodium in komatiites: Evidence for iridium alloy saturation. *Chem. Geol.* **257**, 44–58.

Barnes S. J. and Roeder P. L. (2001) The range of spinel compositions in terrestrial mafic and ultramafic rocks. *J. Petrol.* **42**, 2279–2302.

Barnes S. J., Mungall J. E. and Maier W. D. (2015) Platinum group elements in mantle melts and mantle samples. *Lithos* **232**, 395–417.

Barnes S.-J., Prichard H. M., Cox R. A., Fisher P. C. and Godel B. (2008) The location of the chalcophile and siderophile elements in platinum-group element ore deposits (a textural, microbeam and whole rock geochemical study): Implications for the fortnation of the deposits. *Chem. Geol.* **248**, 295–317.

Barnes S.-J., Page P., Prichard H. M., Zientek M. L. and Fisher P. C. (2016) Chalcophile and platinum-group element distribution in the Ultramafic series of the Stillwater Complex, MT, USA-implications for processes enriching chromite layers in Os, Ir, Ru, and Rh. *Miner Deposita* **51**, 25–47.

Bordage A., Balan E., de Villiers J. P. R., Cromarty R., Juhin A., Carvallo C., Calas G., Raju P. V. S. and Glatzel P. (2011) V oxidation state in Fe-Ti oxides by high-energy resolution fluorescence-detected X-ray absorption spectroscopy. *Phys. Chem. Miner.* **38**, 449–458.

Brenan J. M. and Andrews D. (2001) High-temperature stability of laurite and Ru-Os-lr alloy and their role in PGE fractionation in mafic magmas. *Can Mineral.* **39**, 341–360.

Borisov, A., Nachtweyh, K., 1998. Ru solubility in silicate melts: experimental results in oxidizing region. Lunar and Planetary Science XXIX, abstract no. 1320.

Borisov A. and Palme H. (1995) The solubility of iridium in silicate melts - New data from experiments with Ir10pt90 Alloys. *Geochim. Cosmochim. Acta* **59**, 481–485.

Brenan J. M., Finnigan C. F., McDonough W. F. and Homolova V. (2012) Experimental constraints on the partitioning of Ru, Rh, Ir, Pt and Pd between chromite and silicate melt: The importance of ferric iron. *Chem. Geol.* **302**, 16–32.

Brenan J. M., McDonough W. F. and Ash R. (2005) An experimental study of the solubility and partitioning of iridium, osmium and gold between olivine and silicate melt. *Earth Planet. Sci. Lett.* **237**, 855–872.

Brenan J. M., McDonough W. F. and Dalpe C. (2003) Experimental constraints on the partitioning of rhenium and some platinum-group elements between olivine and silicate melt. *Earth Planet. Sci. Lett.* **212**, 135–150.

Burns R. G. and Fyfe W. S. (1964) Site of preference energy + selective uptake of transition-metal ions from magma. *Science* **144**, 1001–1003.

Cameron W. E. (1985) Petrology and origin of primitive lavas from the Troodos Ophiolite. *Cyprus. Contrib. Mineral. Petrol.* **89**, 239–255.

Capobianco C. J. and Drake M. J. (1990) Partitioning of ruthenium, rhodium, and palladium between spinel and silicate melt and implications for platinum group element fractionation trends. *Geochim. Cosmochim. Acta* **54**, 869–874.

Capobianco C. J. and Drake M. J. (1994) Partitioning and solubility of PGEs in oxides and silicates. *Mineral. Mag.* **58A**, 144–145.

Dale C. W., Macpherson C. G., Pearson D. G., Hammond S. J. and Arculus R. J. (2012) Inter-element fractionation of highly siderophile elements in the Tonga Arc due to flux melting of a depleted source. *Geochim. Cosmochim. Acta* **89**, 202–225.

Dilek Y. and Furnes H. (2011) Ophiolite genesis and global tectonics: Geochemical and tectonic fingerprinting of ancient oceanic lithosphere. *Geol. Soc. Am. Bull.* **123**, 387–411.

Eggins S. M. (1993) Origin and differentiation of picritic arc magmas, Ambae (Aoba), Vanuatu. *Contrib. Mineral. Petrol.* **114**, 79–100.

Ertel W., O'Neill H. S., Sylvester P. J. and Dingwell D. B. (1999) Solubilities of Pt and Rh in a haplobasaltic silicate melt at 1300 degrees C. *Geochim. Cosmochim. Acta* **63**, 2439–2449.

Finnigan C. S., Brenan J. M., Mungall J. E. and McDonough W. F. (2008) Experiments and models bearing on the role of chromite as a collector of platinum group minerals by local reduction. *J. Petrol.* **49**, 1647–1665.

Fiorentini M. L., Stone W. E., Beresford S. W. and Barley M. E. (2004) Platinum-group element alloy inclusions in chromites from Archaean mafic-ultramafic units: evidence from the Abitibi and the Agnew-Wiluna Greenstone Belts. *Mineral. Petrol.* **82**, 341–355.

Fortenfant S. S., Dingwell D. B., Ertel-Ingrisch W., Capmas F., Birck J. L. and Dalpe C. (2006) Oxygen fugacity dependence of Os solubility in haplobasaltic melt. *Geochim. Cosmochim. Acta* **70**, 742–756.

Geschwind S. and Remeika J. P. (1962) Spin resonance of transition metal ions in corundum. *J. Appl. Phys.* **33**, 370–377.

Gonzalez-Jimenez J. M., Griffin W. L., Proenza J. A., Gervilla F., O'Reilly S. Y., Akbulut M., Pearson N. J. and Arai S. (2014) Chromitites in ophiolites: How, where, when, why? Part II. The crystallisation of chromitites. *Lithos* **189**, 140–158.

Hamlyn P. R., Keays R. R., Cameron W. E., Crawford A. J. and Waldron H. M. (1985) Precious metals in magnesian Low-Ti Lavas - Implications for metallogenesis and sulfur saturation in primary magmas. *Geochim. Cosmochim. Acta* **49**, 1797–1811.

Hanski E., Kamenetsky V. S., Luo Z. Y., Xu Y. G. and Kuzmin D. V. (2010) Primitive magmas in the Emeishan Large Igneous Province, southwestern China and northern Vietnam. *Lithos* **119**, 75–90.

Hanski E. and Kamenetsky V. S. (2013) Chrome spinel-hosted melt inclusions in Paleoproterozoic primitive volcanic rocks, northern Finland: Evidence for coexistence and mixing of komatiitic and picritic magmas. *Chem. Geol.* **343**, 25–37.

Hanski E., Huhma H., Rastas P. and Kamenetsky V. S. (2001) The Palaeoproterozoic komatiite-picrite association of Finnish Lapland. *J. Petrol.* **42**, 855–876.

Holm P. M., Gill R. C. O., Pedersen A. K., Larsen J. G., Hald N., Nielsen T. F. D. and Thirlwall M. F. (1993) The Tertiary picrites of West Greenland - Contributions from Icelandic and other sources. *Earth Planet. Sci. Lett.* **115**, 227–244.

Husen A., Kamenetsky V. S., Everard J. L. and Kamenetsky M. B. (2016) Transition from ultra-enriched to ultra-depleted primary MORB melts in a single volcanic suite (Macquarie Island, SW Pacific): Implications for mantle source, melting process and plumbing system. *Geochim. Cosmochim. Acta* **185**, 112–128.

Ireland T. J., Walker R. J. and Garcia M. O. (2009) Highly siderophile element and Os-187 isotope systematics of Hawaiian picrites: Implications for parental melt composition and source heterogeneity. *Chem. Geol.* **260**, 112–128.

Jochum K. P., Weis U., Stoll B., Kuzmin D., Yang Q. C., Raczek I., Jacob D. E., Stracke A., Birbaum K., Frick D. A., Gunther D. and Enzweiler J. (2011) Determination of reference values for NIST SRM 610–617 glasses following ISO guidelines. *Geostand. Geoanal. Res.* **35**, 397–429.

Kamenetsky V. S. (1996) Methodology for the study of melt inclusions in Cr-spinel, and implications for parental melts of MORB from FAMOUS area. *Earth Planet. Sci. Lett.* **142**, 479–486.

Kamenetsky V. S. and Crawford A. J. (1998) Melt-peridotite reaction recorded in the chemistry of spinel and melt inclusions in basalt from 43 degrees N, Mid-Atlantic Ridge. *Earth Planet. Sci. Lett.* **164**, 345–352.

Kamenetsky V. S., Chung S. L., Kamenetsky M. B. and Kuzmin D. V. (2012) Picrites from the Emeishan Large Igneous Province, SW China: a compositional continuum in primitive magmas and their respective mantle sources. *J. Petrol.* **53**, 2095–2113.

Kamenetsky V. S. and Eggins S. M. (2012) Systematics of metals, metalloids, and volatiles in MORB melts: Effects of partial melting, crystal fractionation and degassing (a case study of Macquarie Island glasses). *Chem. Geol.* **302**, 76–86.

Kamenetsky V. S., Maas R., Fonseca R. O. C., Ballhaus C., Heuser A., Brauns M., Norman M. D., Woodhead J. D., Rodemann T., Kuzmin D. V. and Bonatti E. (2013) Noble metals potential of sulfide-saturated melts from the subcontinental lithosphere. *Geology* **41**, 575–578.

Kamenetsky V. S., Crawford A. J. and Meffre S. (2001) Factors controlling chemistry of magmatic spinel: An empirical study of associated olivine, Cr-spinel and melt inclusions from primitive rocks. *J. Petrol.* **42**, 655–671.

Kamenetsky V. S., Park J.-W., Mungall J. E., Pushkarev E. V., Ivanov A. V., Kamenetsky M. B. and Yaxley G. M. (2015) Crystallization of platinum-group minerals from silicate melts: Evidence from Cr-spinel-hosted inclusions in volcanic rocks. *Geology* **43**, 903–906.

Kamenetsky V. S., Sobolev A. V., Joron J. L. and Semet M. P. (1995) Petrology and geochemistry of Cretaceous ultramafic volcanics from Eastern Kamchatka. *J. Petrol.* **36**, 637–662.

Kepezhinskas P., Defant M. J. and Widom E. (2002) Abundance and distribution of PGE and Au in the island-arc mantle: implications for sub-arc metasomatism. *Lithos* **60**, 113–128.

Kurepin V. A. (2005) A thermodynamic model of Fe-Cr spinels. *Contrib. Mineral. Petrol.* **149**, 591–599.

Langmuir C. H., Bender J. F., Bence A. E., Hanson G. N. and Taylor S. R. (1977) Petrogenesis of basalts from Famous area - Mid-Atlantic Ridge. *Earth Planet. Sci. Lett.* **36**, 133–156.

Larsen L. M. and Pedersen A. K. (2000) Processes in high-mg, high-T magmas: Evidence from olivine, chromite and glass in palaeogene picrites from West Greenland. *J. Petrol.* **41**, 1071–1098.

Li C. S., Tao Y., Qi L. and Ripley E. M. (2012) Controls on PGE fractionation in the Emeishan picrites and basalts: Constraints from integrated lithophile-siderophile elements and Sr-Nd isotopes. *Geochim. Cosmochim. Acta* **90**, 12–32.

Lissner M., Konig S., Luguet A., le Roux P. J., Schuth S., Heuser A. and le Roex A. P. (2014) Selenium and tellurium systematics in MORBs from the southern Mid-Atlantic Ridge (47–50 degrees S). *Geochim. Cosmochim. Acta* **144**, 379–402.

Locmelis M., Pearson N. J., Barnes S. J. and Fiorentini M. L. (2011) Ruthenium in komatiitic chromite. *Geochim. Cosmochim. Acta* **75**, 3645–3661.

Longerich H. P., Jackson S. E. and Gunther D. (1996) Laser ablation inductively coupled plasma mass spectrometric transient signal data acquisition and analyte concentration calculation. *J. Anal. Atom. Spectrom.* **11**, 899–904.

Mallmann G. and O'Neill H. S. C. (2009) The Crystal/Melt Partitioning of V during Mantle Melting as a Function of Oxygen Fugacity Compared with some other Elements (Al, P, Ca, Sc, Ti, Cr, Fe, Ga, Y, Zr and Nb). *J. Petrol.* **50**, 1765–1794.

Mattioli G. S. and Wood B. J. (1988) Magnetite activities across the $MgAl_2O_4$-Fe_3O_4 spinel join, with application to thermobarometric estimates of upper mantle oxygen fugacity. *Contrib. Mineral. Petrol.* **98**, 148–162.

McDonough W. F. and Sun S. S. (1995) The composition of the Earth. *Chem. Geol.* **120**, 223–253.

Meisel T., Fellner N. and Moser J. (2003) A simple procedure for the determination of platinum group elements and rhenium (Ru, Rh, Pd, Re, Os Ir and Pt) using ID-ICP-MS with an inexpensive on-line matrix separation in geological and environmental materials. *J. Anal. Atom. Spectrom.* **18**, 720–726.

Nell J., Wood B. J. and Mason T. O. (1989) High-temperature cation distributions in Fe_3O_4-$MgAl_2O_4$-$MgFe_2O_4$-$FeAl_2O_4$ spinels from thermopower and conductivity measurements. *Am. Mineral.* **74**, 339–351.

Niu Y. L., Wilson M., Humphreys E. R. and O'Hara M. J. (2011) The Origin of Intra-plate Ocean Island Basalts (OIB): the Lid Effect and its Geodynamic Implications. *J. Petrol.* **52**, 1443–1468.

Page N. J., Engin T., Singer D. A. and Haffty J. (1984) Distribution of platinum-group elements in the Bati-Kef chromite deposit, Guleman-Elazig Area, Eastern Turkey. *Econ. Geol.* **79**, 177–184.

Pagé P., Barnes S.-J., Bédard J. H. and Zientek M. L. (2012) *In situ* determination of Os, Ir, and Ru in chromites formed from komatiite, tholeiite and boninite magmas: Implications for chromite control of Os, Ir and Ru during partial melting and crystal fractionation. *Chem. Geol.* **302–303**, 3–15.

Pagé P. and Barnes S.-J. (2009) Using trace elements in chromites to constrain the origin of podiform chromitites in the Thetford Mines Ophiolite, Quebec, Canada. *Econ. Geol.* **104**, 997–1018.

Pagé P. and Barnes S.-J. (2016) The influence of chromite on osmium, iridium, ruthenium and rhodium distribution during early magmatic processes. *Chem. Geol.* **420**, 51–68.

Park J.-W., Campbell I. H. and Arculus R. J. (2013) Platinum-alloy and sulfur saturation in an arc-related basalt to rhyolite suite: evidence from the Pual Ridge lavas, the Eastern Manus Basin. *Geochim. Cosmochim. Acta* **101**, 76–95.

Park J.-W., Campbell I. H. and Eggins S. M. (2012) Enrichment of Rh, Ru, Ir and Os in Cr spinels from oxidized magmas: evidence from the Ambae volcano, Vanuatu. *Geochim. Cosmochim. Acta* **78**, 28–50.

Park J.-W., Campbell I. H. and Kamenetsky V. (2015a) The role of Cr-spinel crystallization on platinum group elememt fractionation in terrestrial magmas. *Goldschmidt Abstracts* **2015**, 2408.

Park J.-W., Campbell I. H., Kim J. and Moon J. W. (2015b) The role of late sulfide saturation in the formation of a Cu- and Au-rich magma: Insights from the platinum group element geochemistry of Niuatahi-Motutahi lavas, Tonga Rear Arc. *J. Petrol.* **56**, 59–81.

Parkinson I. J. and Pearce J. A. (1998) Peridotites from the Izu-Bonin-Mariana forearc (ODP leg 125): Evidence for mantle melting and melt-mantle interaction in a supra-subduction zone setting. *J. Petrol.* **39**, 1577–1618.

Peach C. L., Mathez E. A. and Keays R. R. (1990) Sulfide melt-silicate melt distribution coefficients for noble metals and other chalcophile elements as deduced from MORB: Implications for partial melting. *Geochim. Cosmochim. Acta* **54**, 3379–3389.

Philipp H., Eckhardt J. D. and Puchelt H. (2001) Platinum-group elements (PGE) in basalts of the seaward-dipping reflector sequence, SE Greenland coast. *J. Petrol.* **42**, 407–432.

Prichard H. M., Barnes S. J., Dale C. W., Godel B., Fisher P. C. and Nowell G. M. (2017) Paragenesis of multiple platinum-group mineral populations in Shetland ophiolite chromitite: 3D X-ray tomography and in situ Os isotopes. *Geochim. Cosmochim. Acta* **216**, 314–334.

Righter K., Campbell A. J., Humayun M. and Hervig R. L. (2004) Partitioning of Ru, Rh, Pd, Re, Ir, and Au between Cr-bearing spinel, olivine, pyroxene and silicate melts. *Geochim. Cosmochim. Acta* **68**, 867–880.

Roeder P., Gofton E. and Thornber C. (2006) Cotectic proportions of olivine and spinel in olivine-tholeiitic basalt and evaluation of pre-eruptive processes. *J. Petrol.* **47**, 883–900.

Shibata T., Thompson G. and Frey F. A. (1979) Tholeiitic and alkali basalts from the Mid-Atlantic Ridge at 43-degrees-N. *Contrib. Mineral. Petrol.* **70**, 127–141.

Sutton S. R., Karner J., Papike J., Delaney J. S., Shearer C., Newville M., Eng P., Rivers M. and Dyar M. D. (2005) Vanadium K edge XANES of synthetic and natural basaltic glasses and application to microscale oxygen barometry. *Geochim. Cosmochim. Acta* **69**, 2333–2348.

Sylvester P. J. and Eggins S. M. (1997) Analysis of Re, Au, Pd, Pt and Rh in NIST glass certified reference materials and natural basalt glasses by laser ablation ICP-MS. *Geostandard Newslett.* **21**, 215–229.

Tredoux M., Lindsay N. M., Davies G. and McDonald I. (1995) The fractionation of platinum-group elements in magmatic systems, with the suggestion of a novel causal mechanism. *South Afr. J. Geol.* **98**, 157–167.

Wißmann S., Von Wurmb V., Litterst F. J., Dieckmann R. and Becker K. D. (1998) The temperature-dependent cation distribution in magnetite. *J. Phys. Chem. Solids* **59**, 321–330.

Woodland S. J., Pearson D. G. and Thirlwall M. F. (2002) A platinum group element and Re-Os isotope investigation of siderophile element recycling in subduction zones: Comparison of Grenada, Lesser Antilles arc, and the Izu-Bonin arc. *J. Petrol.* **43**, 171–198.

Xu Y. G., Chung S. L., Jahn B. M. and Wu G. Y. (2001) Petrologic and geochemical constraints on the petrogenesis of Permian-Triassic Emeishan flood basalts in southwestern China. *Lithos* **58**, 145–168.

Yang A. Y., Zhou M. F., Zhao T. P., Deng X. G., Qi L. and Xu J. F. (2014) Chalcophile elemental compositions of MORBs from the ultraslow-spreading Southwest Indian Ridge and controls of lithospheric structure on S-saturated differentiation. *Chem. Geol.* **382**, 1–13.

Zhang S. X., Wu S. Y., Xu P. and Li L. L. (2010) Theoretical investigations on the spin Hamiltonian parameters and the local structure for Rh^{2+} in rutile. *Can. J. Phys.* **88**, 49–53.

Zhang Z. C., Mao J. W., Mahoney J. J., Wang F. S. and Qu W. J. (2005) Platinum group elements in the Emeishan large igneous province, SW China: Implications for mantle sources. *Geochem. J.* **39**, 371–382.

Zhou M. F., Robinson P. T. and Bai W. J. (1994) Formation of podiform chromitites by melt rock interaction in the upper-mantle. *Miner. Deposita* **29**, 98–101.

Associate editor: Christopher W. Dale